KINETICS OF IRON OXIDE REDUCTION AND STUDY OF EMULSION FORMATION IN STEELMAKING

A Thesis Submitted

in Partial Fulfillment of the Requirement

for the Degree of

MASTER OF TECHNOLOGY

by

AMITAVA PAUL

to the

DEPARTMENT OF MATERIALS AND METALLURGICAL ENGINEERING

INDIAN INSTITUTE OF TECHNOLOGY KANPUR

JULY 1994

MME-1994-M-PAU-KIN

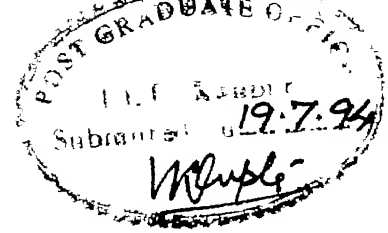

CERTIFICATE

It is certified that the work contained in the thesis entitled "*Kinetics of Iron Oxide Reduction and Study of Emulsion Formation in Steelmaking*", by Amitava Paul, has been carried out under my supervision and that this work has not been submitted elsewhere for a degree.

Dr. Brahma Deo

Professor

Department of Materials and Metallurgical Engineering

Indian Institute of Technology Kanpur

July 1994

ACKNOWLEDGEMENT

It is a matter of immense pleasure for me to express my heartfelt gratitude to my thesis supervisor Prof. Brahma Deo who had been inspiring and guiding me from starting of the project.

I am thankful to Prof. A. Ghosh, Prof. N. Sathyamurthy and Prof. R. Shekhar for their useful suggestions regarding my project work.

Special thanks are owed to Mr. Joydev Mukherjee and Mr. K.S. Rao for the useful discussions we had time to time.

I express my heartfelt gratitude to my friends Amlan, Pranabesh, Vidya, Sunita and Lalu for boosting up my morale and helping me to take decisions.

I am grateful to all the members of 'Labango Latika' and 'Hall 5, C-Top' who made my life enjoyable at I. I. T. Kanpur.

Lastly I thank all those who directly or indirectly helped me to complete my thesis.

Amitava Paul

SYNOPSIS

Rate of reduction of iron oxide in iron and steelmaking slags by dissolved carbon (>3 wt%) in molten iron depends upon activity of FeO, temperature, mixing of bulk slag and other experimental conditions. A general kinetic model is developed by considering mass transfer of FeO in slag, chemical reaction at gas-metal interface and chemical reaction at gas-slag interface, respectively, as the three rate controlling steps. A critical analysis of the experimental data reported in literature has been done. The temperature dependence of rate constant for the gas-slag reaction is obtained as

$$\ln k_2 = -32{,}345.4(\pm 6{,}128)/T + 19.0(\pm 3.42);\ \sigma_{\ln k_2,\,1/T} = \pm 0.3$$

where k_2 is expressed in mol $m^{-2}s^{-1}bar^{-1}$

The mass transfer coefficient of iron oxide in bulk slag is found to vary in the range 1.5×10^{-5} to 5.0×10^{-5} m/s, depending upon the slag composition as well as experimental conditions.

Metal droplets of various sizes are ejected from the jet impact area in oxygen steelmaking converters. The residence time of these droplets in the surrounding gas bubble-slag mixture is calculated for different operating conditions in top blown converters. A new dimensionless emulsion number, En, based on the ratio of the residence time of metal droplets to the residence time of gas bubbles in liquid slag is proposed. The reduction of FeO in slag by dissolved carbon in metal droplets also depends on emulsion number. Since FeO contents of slag decides lime dissolution, slopping and lining dissolution, the emulsion can be used as an effective tool to control slag formation behavior.

TABLE OF CONTENTS

List of Figures

indicated. Hatched region in (a) shows transition zone from Model-I to Model-II and hatched region in (b) shows transition zone from Model-II to Model-III.

Fig. 2.3 Resistances offered by various rate controlling steps at different FeO content of slags: (a) Actual resistances vs. FeO content (b) Relative resistances vs. FeO content; dotted lines are extrapolated.

Fig. 3.1 Specific iron conversion versus Weber number [38].

Fig. 3.2 Variation of iron conversion (Mg) with lance height for three different plants (nozzle designs are same as given in Table 3.1)

Fig. 3.3 Emulsion number at different ratios of (x/d_t) (lance height to nozzle throat diameter); gas fractions (ϕ_g) varied between 0.1 to 0.9; nozzle design same as that for Plant B in Table 3.1.

Fig. 3.4 a) Blowing regime (lance height at different times during a blow) practiced at Plants A, B, and C of (Table 3.1)

b) Emulsion number versus process time for Plants A, B, and C (Table 3.1); for $\phi_g = 0.7$.

Fig. 3.5 Variation of Emulsion number with lance height for three different nozzle designs (Plants A, B, and C in Table 1); for $\phi_g = 0.7$.

Fig. 3.6 Variation of Emulsion number with supply pressure of oxygen for three different lance heights with $\phi_g = 0.7$; nozzle design is same as that of Plant B in Table 3.1.

Fig. 3.7 Plot of reduction rate of FeO by metal droplets versus lance height at different gas fractions ϕ_g.

Fig. 3.8 a) Variation of reduction rate of FeO with Emulsion number

List of Tables

LIST OF SYMBOLS

a_{Fe}	Activity of iron (=1)
a^{i}_{FeO}	Activity of FeO at gas-slag interface [dimensionless]
A	Total reaction surface area of metal droplets [m^2]
A_e	Cross sectional area of nozzle at exit [m^2]
A_t	Cross sectional area of nozzle at throat [m^2]
C^{b}_{FeO}	Concentration of FeO in the bulk of the slag [mol/m^3]
C^{i}_{FeO}	Concentration of FeO at the gas-slag interface [mol/m^3]
d_{avg}	Average metal droplet diameter [m]
d_b	Diameter of a bubble [m]
d_{bcr}	Critical diameter of bubbles [m]
d_e	Exit diameter of nozzle [m]
d_{llm}	Upper limiting size of metal droplets [m]
d_m	Diameter of a droplet [m]
d_t	Throat diameter for a lance nozzle [m]
D^{s}	Diffusivity of surfactant [m^2s^{-1}]
En	Emulsion Number [dimensionless]
f(d)	Droplet size distribution [dimensionless]
F_{O_2}	Oxygen flow rate [m^3s^{-1}]
FeO_o	Initial concentration of FeO in slag [wt%]
FeO_t	Concentration of FeO in slag after time t [wt%]
h	Foam height [m]
k_2	Forward reaction rate constant of FeO + CO = Fe + CO_2, [$molm^{-2}s^{-1}bar^{-1}$],
k_{3a}	Reaction rate constant for dissociative chemisorption of CO_2 (CO_2 = CO + [O]) [$molm^{-2}s^{-1}bar^{-1}$],
K	Equilibrium constant of reaction FeO + CO = Fe + CO_2,

MO_2	Molecular weight of oxygen [kg $kmol^{-1}$]
Mg	Iron conversion [kg s^{-1}]
n	Number of holes in the nozzle
n_{CO}	Number of moles of CO gas [mol]
n_{CO2}	Number of moles of CO_2 gas [mol]
n_{FeO}	Number of moles of FeO in slag [mol]
n_{tot}	Total number of moles of slag [mol]
p_a	Ambient Pressure [bar]
p_{CO}	Partial pressure of CO in gas phase [bar]
p_{CO2}	Partial pressure of CO_2 [bar]
p_e	Pressure of jet at nozzle exit [bar]
p_o	Supply pressure of O_2 to lance [bar]
r	Retardation coefficient due to presence of surfactant (as defined in Ref. [25])
R_u	Universal gas constant [J mol^{-1} K^{-1}]
t	Time [s]
t_{avg}	Mean residence time of metal droplets in slag [s]
t_g	Mean residence time of gas bubbles in slag [s]
t_r	Residence time of a metal droplet [s]
T_o	Stagnant temperature of oxygen jet [K]
T	Temperature [K]
u_e	Velocity of jet at nozzle exit [ms^{-1}]
$u_{o,x}$	Center line velocity of jet at distance x from nozzle [ms^{-1}]
V_g	Rising velocity of gas bubbles in slag [ms^{-1}]
V_d	Settling velocity of metal droplets in gas-slag mixture [ms^{-1}]
Vl_i	Volume of phase i [m^3]
We	Weber number [dimensionless]
Ws	Weight of slag [kg]

x	Lance height [m]

Greek Symbols

α^*	Overall adsorption rate constant
β	Nozzle constant [dimensionless]
β_o	Constant of adsorption kinetics
γ	Adiabatic gas constant [dimensionless]
γ_{FeO}	Activity coefficient of FeO in slag [dimensionless]
Γ	Surface concentration of surfactant
Γ_o	Equilibrium surface concentration of surfactant
ξ	Friction factor [dimensionless]
θ	Angle of the divergent part of the nozzle [radian]
δ	Thickness of boundary layer of diffusion [m]
μ_i	Viscosity of phase i [kg $m^{-1}s^{-1}$]
ρ_i	Density of phase i [kg m^{-3}]
σ_i	Surface tension of phase i [kg s^{-2}]
ϕ_i	Volume fraction of phase i in gas-metal-slag emulsion [dimensionless]
ζ	Retardation constant (as defined in Ref. [25])

subscripts

c	Continuum phase
d	Dispersed phase
g	Gas phase
m	Metal phase
s	Slag phase
sm	Slag-metal continuum phase
sg	Slag-gas continuum phase
eff	Effective values of emulsion properties (same as 'sg')

CHAPTER 1

GENERAL ASPECTS OF FeO REDUCTION AND EMULSION FORMATION IN STEELMAKING SLAGS

1.1 Reduction of Molten Iron Oxide in Slags by Fe-C Melt

The kinetics of reduction of iron oxide by carbon dissolved in iron melt plays an important role in the production of iron and steel by conventional processes as well as by modern smelting reduction processes. For example, in oxygen steelmaking the slag containing 5-15 wt% FeO exists simultaneously with iron-carbon melt and the metal droplets dispersed in slag. Also, in smelting reduction processes, a substantial fraction of the iron oxide in the slag is reduced to molten iron either by carbon particles blown into the metal or by carbon atoms present in dissolved form in molten iron droplets. The overall reaction of FeO with carbon in the melt is a three phase reaction involving slag, metal and gas

$$(FeO) + [C] = \{Fe\} + (CO)_g \qquad (1.1)$$

Since three phases can meet simultaneously only across a line, reaction (1.1) proceeds in two separate steps:
at the gas-slag interface

$$(FeO) + (CO)_g = \{Fe\} + (CO_2)_g \qquad (1.2)$$

and at the gas-metal interface

$$(CO_2)_g + [C] \rightarrow 2\ (CO)_g \qquad (1.3)$$

The fact that reactions (1.2) and (1.3) take place sequentially is proven by laboratory experiments [1-2] which have shown that as soon

as the slag containing FeO comes into contact with metal containing dissolved carbon a $CO-CO_2$ gas film forms at the interface separating the slag and metal. On the basis of reactions (1.2) and (1.3) various steps of reduction of FeO by carbon dissolved in iron can be written as:

Step 1: Transport of carbon in the iron melt to the gas-metal interface.

Step 2: Chemical reaction at the gas-metal interface (Eq. 1.3).

Step 3: Transport of gas from the gas-metal interface to gas-slag interface and vice versa.

Step 4: Transport of iron oxide in the slag to the gas-slag interface.

Step 5: Chemical reaction at the gas-slag interface (Eq. 1.2).

It is clear that, among all these steps, the slowest will determine the overall rate of reduction.

1.1.1 Review of the Previous Work

Several experiments have been reported in the literatures on the kinetics of reduction of FeO in slags by employing CO/CO_2 gas mixtures separately or CO/CO_2 generated by insitu reduction of FeO by carbon dissolved in molten iron. In the latter case CO and CO_2 gases are produced/consumed at the gas-slag-metal interfaces simultaneously.

Sommerville *et al.* [3] measured the rate of reduction iron oxide in slags (containing 1-3 wt% FeO) by carbon dissolved in molten iron. Master slag was of the composition 38 wt% CaO-20 wt% Al_2O_3-42 wt% SiO_2 at around 1400°C. The reduction rate of FeO was measured from rate of evolution of CO gas. The experimental results are plotted in Fig.(1.1) and also summarized in Table 1.1. For slags containing less than 2.5 wt% FeO the reaction rate was found to be

governed by the chemical reaction at gas-metal interface (Eq. (1.3))and the rate equation was given by

$$-Fe\frac{FeO_t - FeO_{eq}}{FeO_o - FeO_{eq}} = \frac{k_3 K\ (1-\theta)\ p_{CO} t}{1} \qquad (1.4)$$

where Fe is concentration in wt% of iron in the melt, k_3 is reaction rate constant (reaction (1.3)), K is equilibrium constant at the experimental temperature (for reaction (1.2)), p_{CO} is equilibrium partial pressure of CO gas (for reaction (1.2)), $(1-\theta)$ is fraction of vacant sites for adsorption of oxygen, FeO is concentration in wt% of FeO in the slag and the subscripts o, t and eq represent values at t = 0, t = t and at equilibrium, respectively.

Table 1.1 Results of reduction of FeO in slag by Fe-C melt [3]

Temp. Time (min)	1390-95 °C	1380-85 °C	1375-80 °C
0	1.53	2.50	3.17
1	1.412	2.393	3.084
2	1.327	2.275	2.988
3	1.273	2.158	2.817
4	1.198	2.051	2.635
5	1.134	1.933	2.41
6	1.059	1.826	2.314
7	0.984	1.751	2.23
8	0.92	1.665	2.152
9	0.877	1.601	2.058
10	0.845	1.537	1.97

Hasham *et al.* [4] investigated the reduction of iron oxide

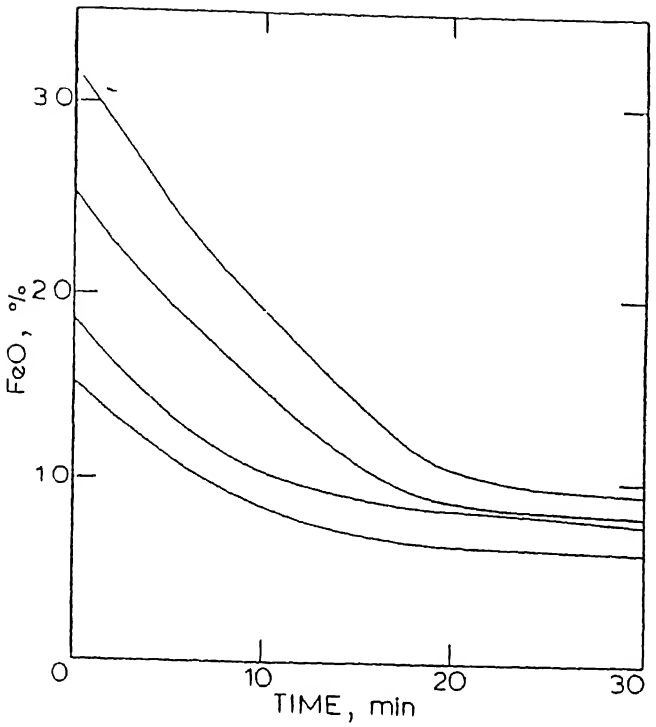

Fig. 1.1 Rate curves for four initial concentrations of FeO [3].

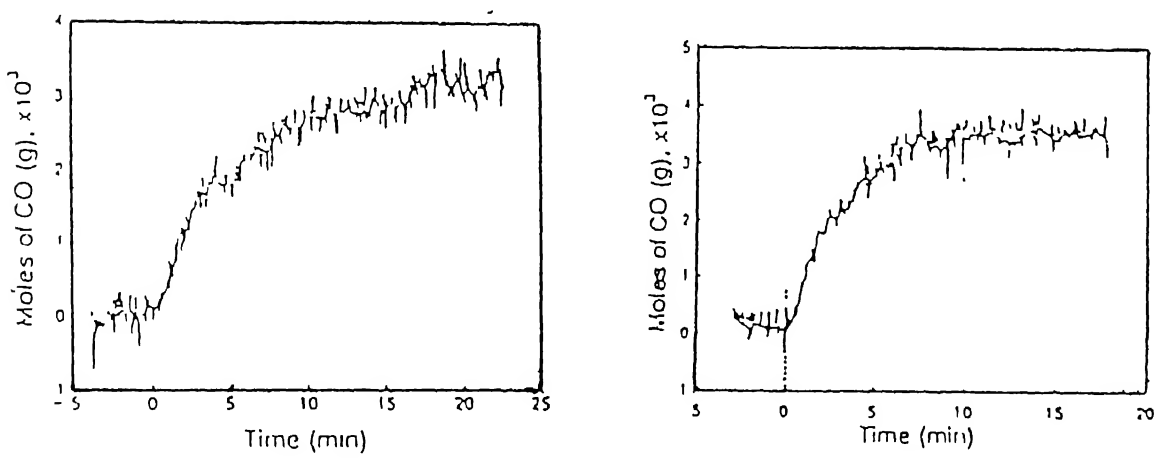

Fig. 1.2 Evolution of CO(g) as a function time during reaction for (a) single Fe-C droplet (b) five Fe-C droplets [4].

dissolved in $CaO-SiO_2-Al_2O_3$ slags by Fe-C melt at 1723 K by conducting two types of experiments: (i) dropping one (or several) Fe-C droplet (s) (weighing 2g) into molten slag bath and (ii) dropping a small amount (10-30g) of slag onto a Fe-C melt weighing 400g. The rate of reduction was monitored by measuring the rate of evolution of CO gas (Fig. (1.2)). It was found that neither the carbon transport in the Fe-C melt nor the transport of gas species in the gas film was responsible for controlling the reduction rate. In the initial stages of reduction mass transport of FeO was suggested as the rate controlling step. However, as soon as the carbon in the droplets fell to about 2-3 wt% some type charge build up in the slag layer (adjacent to the Fe-C melt) was proposed to be responsible for limiting the rate of reduction.

In another work with iron-carbon droplets and slags, Saweda *et al.* [5] concluded that during the first one minute the reduction rate followed zeroth order rate kinetics with respect to carbon in the droplets and first order rate kinetics with respect to FeO in the slag. The relationship between the reduction rate, r, and FeO (wt%) of slag was given as

$$\ln r \text{ (mol-O/s cm}^2\text{)} = 1.114\text{x}10^{-5} + 8.351\text{x}10^{-2} \text{ (\%FeO)} \qquad (1.5)$$

The activation energy, E, was in the range 221-237 KJ/mol-O. They also observed that the reaction virtually stopped when the carbon in the droplets fell below 2-2.5%.

Hacioglu and Pomfret [6] studied kinetics of reduction of iron oxide in slags by iron-carbon melt and concluded that reduction rate was controlled by dissociation of ferrous oxide at the slag surface. This is in contradiction with the results of Sommerville *et*

al. [3].

Sato *et al.* [7-8] employed both pure molten iron oxide [7] and slags containing iron oxide [8]. Experimental results are shown in Fig (1.3). It was found that the rate of reduction of molten iron oxide by the carbon dissolved in molten iron was greater than the reduction rate of molten iron oxide by the solid carbon, or by reducing gases such as CO, H_2 etc. The observed rate of reduction molten iron oxide (50g) by the carbon in molten iron was approximately $1.1\text{-}3.3\text{x}10^{-4}$ mol-FeO/cm^2 s in the temperature range 1420-1620°C and the activation energy of the reaction was found to be 44 kcal/mol. The reduction rate was found to increase with the amount of molten iron oxide in slag.

Sato *et al.* [8] used a Tammann furnace under a controlled atmosphere at 1520°C to study the rate of reduction of iron oxide in molten slags by carbon dissolved in molten iron. Fig (1.4) shows the crucible arrangement and the addition method of slag-iron oxide powder mixture. The chemical composition of the slag (40g, 2.7 % of metal weight) was 44.2% CaO-45.0% SiO_2-10.8% Al_2O_3 ($CaO/SiO_2 \simeq 1.0$). The rate of reduction of FeO was calculated from the amount of CO gas evolved and by analyzing the FeO content of slag at different times (Fig. (1.5)). It was found that rate of reduction of iron oxide by dissolved carbon in the molten iron and by graphite was proportional to the second power of the iron oxide concentration in the molten slag (except at the start and the end of the experiment). They also observed that the rate constant of the slag-metal reaction in an alumina crucible was less than that in a graphite crucible (apparently due to alumina dissolution into the molten slag from the crucible wall). The maximum value of the rate constant of the reduction of

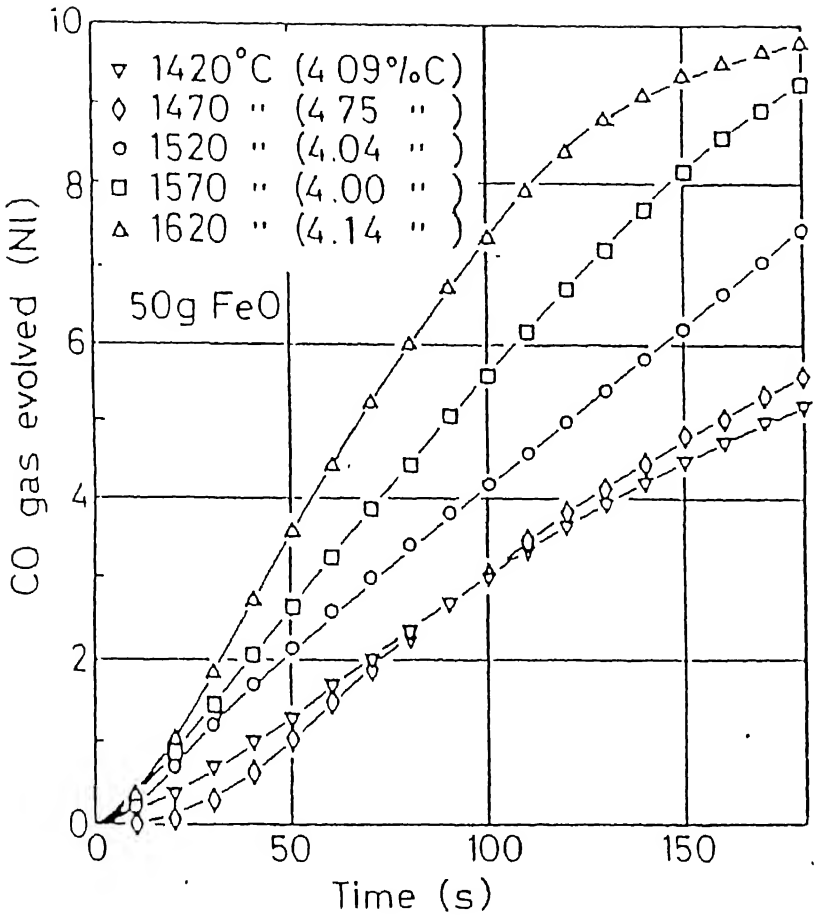

Fig. 1.3 Amount of CO gas evolution versus time during the reduction of molten iron oxide by carbon in molten iron [7].

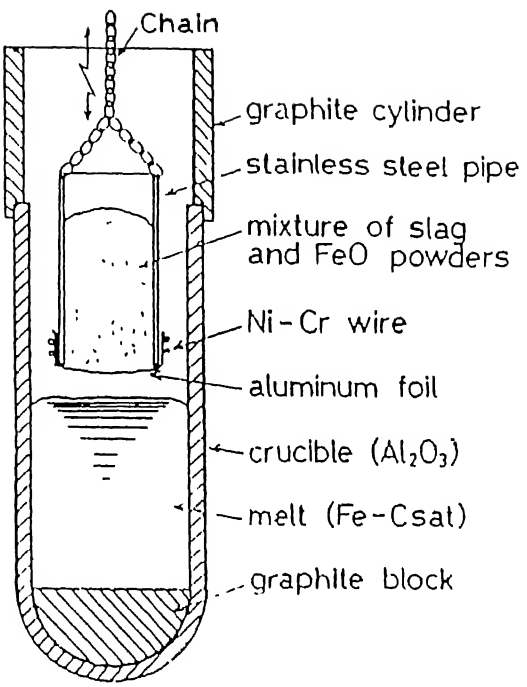

Fig. 1.4 Schematic diagram of the crucible arrangement and the addition method of the master slag and iron oxide powder mixture [8].

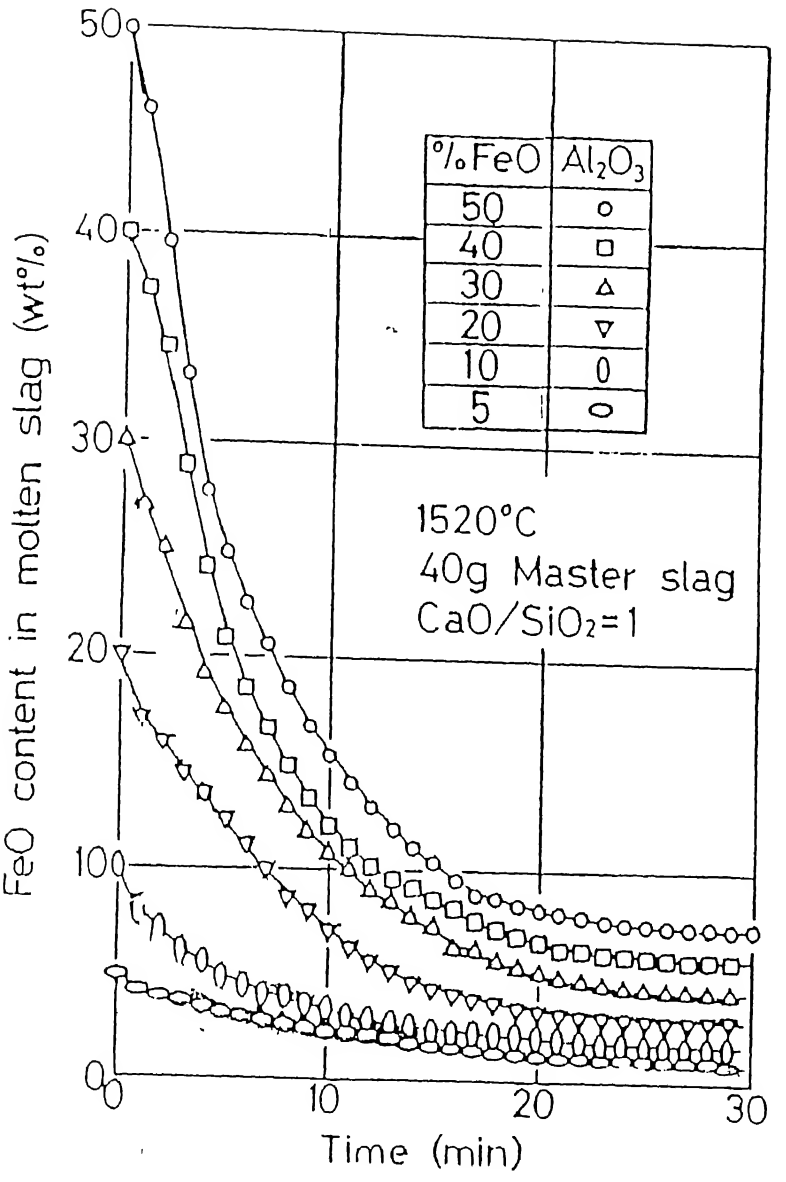

Fig. 1.5 Variation of iron oxide content in molten slag with time for different initial iron oxide contents [8].

iron oxide in the molten slag (by carbon in the molten iron or graphite) was observed approximately at CaO/SiO_2 = 1.5 of molten slag.

Wei and co-investigators [9-10] studied the oxidation of dissolved carbon (4.4 wt%) in a mechanically stirred bath by slags containing iron oxide at 1300°C. They employed special type of primary slags containing CaO, Li_2O, and SiO_2 in the molar ratio of 1:1:1; in other works mostly $CaO-Al_2O_3-SiO_2$ slag was used. Results of their experiments at 200 rpm. are shown in Fig. (1.6) [9]. The kinetic model incorporating the three rate controlling steps namely, chemical reaction at gas-slag interface, CO_2 mass transport in the bubble and chemical reaction at the gas-metal interface was found to fit the data well. Dissolved P in the slag was detrimental to the oxidation of dissolved carbon. Simultaneous oxidation of dissolved silicon in the metal also lowered the oxidation rate of carbon. According to Wai *et al.* [10] at high FeO concentrations the slag phase is stirred by the CO bubbles formed at the slag-metal interface and therefore mechanical stirring had almost no influence on enhancing the mass transfer of FeO in the slag.

Bafghi *et al.* [11] investigated the effect foaming phenomenon on the reduction kinetics of iron oxide present in slag by graphite. The effect of foaming could be incorporated by introducing gas holdup factor in the rate equations. For iron oxide contents between 3-12 wt% the rate of reduction of was controlled by the mass transfer of FeO in the slag phase. In another study Bafghi *et al.* [12] found that reaction rate was significantly affected by slag composition; for slags with basicity of 2 the reaction rate was essentially controlled by mass transfer of FeO in the slag phase; chemical reaction control became predominant only at lower basicities.

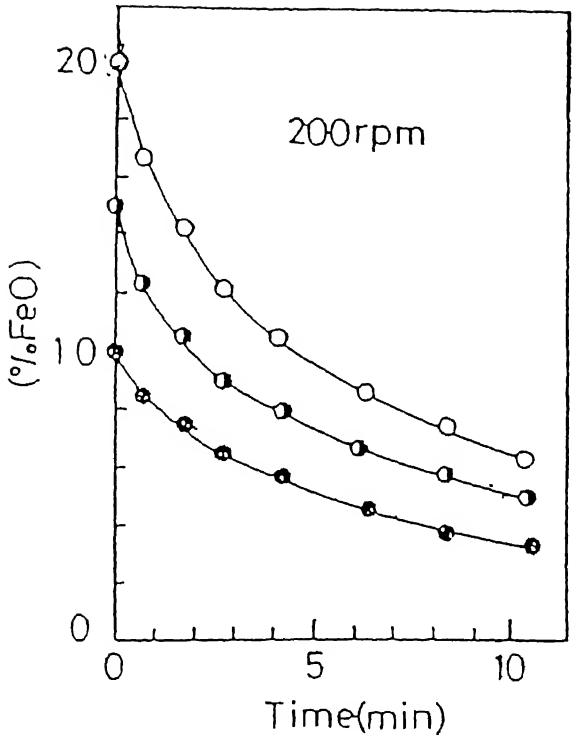

Fig. 1.6 Variation of iron oxide content in molten slag with time for different initial iron oxide contents at a stirring speed 200 rpm [9].

Chemisorption of surface active agents (like silicon and/or phosphorus) at the interface was found to lower the chemical reaction rate.

Sugata *et al.* [13] measured the rate of reduction of iron oxide in molten slags by rotating carbon rod or coke rod in the temperature range of 1350°C to 1450°C. At higher rotation speeds (above 400 rpm.) there was no effect of rotation speed of carbon rod on the reduction rate. It was therefore inferred that the chemical reaction was rate controlling step. The rate equation was given as

$$-\frac{1}{A}\dot{n}_{FeO} = 17.3 \exp\left(-\frac{39700}{RT}\right).a_{FeO} \qquad (1.6)$$

where A is the reaction surface area, $\dot{n}_{FeO}$ is reduction rate of FeO and a_{FeO} is the activity FeO in slag. At lower rotation speeds the rate was found to be controlled by both the diffusion in molten slag and the chemical reaction.

Nagasaka *et al.* [14] and Fine *et al.* [15] studied reduction of molten iron oxide with CO gas. Nagasaka *et al.* [14] measured the reduction rate by using a thermobalance. The effect of mass transfer in the gas and liquid phases on the overall reaction rate was carefully estimated. The experimental results followed the empirical relation:

$$r = \left(\frac{N^2_{Fe^{3+}}}{N^3_{Fe^{2+}}}\right)^{1/3} \left(P_{CO} - \frac{P_{CO2}}{K_C}\right) \exp\left(-\frac{33000}{RT} + 2.86\right) \qquad (1.7)$$

where r is reduction rate, K_C is equilibrium constant of reaction (1.2), and $N_{Fe^{3+}}$ and $N_{Fe^{2+}}$ are mole fractions of Fe^{3+} and Fe^{2+} ions, respectively. Fine *et al.* [15] measured the reduction rate of FeO present in $CaO-SiO_2-MgO$ slags by CO at 1873 K with the help of infrared gas analyzer (by analyzing the amount of CO_2 in exhaust

gases). The reduction rate was found to be independent of FeO concentration for a slag with 67.7-48.0 wt% FeO. However, for slags with less than 48 wt% FeO reduction rate was found to depend on the concentration of FeO and the partial pressure of CO gas.

From the study of reduction of pure solid ferrous oxide and magnetite by molten pig iron, Dancy [16] observed that the reduction of ferrous oxide was faster than that of magnetite at a given temperature but the increase in rate with temperature was similar. It was concluded that the reduction of ferrous oxide was a first-order reaction upto 80% reduction in the temperature range of 1430-1595°C and the reduction of magnetite followed a first-order relation only upto 30% reduction in the temperature range of 1600-1840°C. Apparent activation energy was determined as -43000±4300 cal/mol for FeO and -37300±3700 cal/mol for magnetite.

Sain and Belton [17] studied the kinetics of decarburization of liquid iron saturated with carbon under the conditions where mass transfer was purposely eliminated as the rate determining step by using an inductively stirred melt and a very high gas flow rates. The carbon concentration of iron melt was kept at near saturation level by cementing a graphite block at the bottom of the crucible (Fig (1.7)). The reduction of FeO was found to be controlled by chemisorption of CO_2 (i.e., $CO_2 = CO + \underline{O}$) as a rate controlling step. The rate constant, k_f (in mol $cm^{-2}s^{-1}atm^{-1}$, calculated from $\frac{dC}{dt} = -k_f\ p_{CO_2}$) was given as a function of temperature

$$\ln k_f = -11700/T - 0.48 \qquad (1.8)$$

Mannion and Fruehan [18] also investigated the kinetics of the decarburization of $Fe\text{-}C_{sat}$ liquid alloys by CO_2 gas at 1600°C

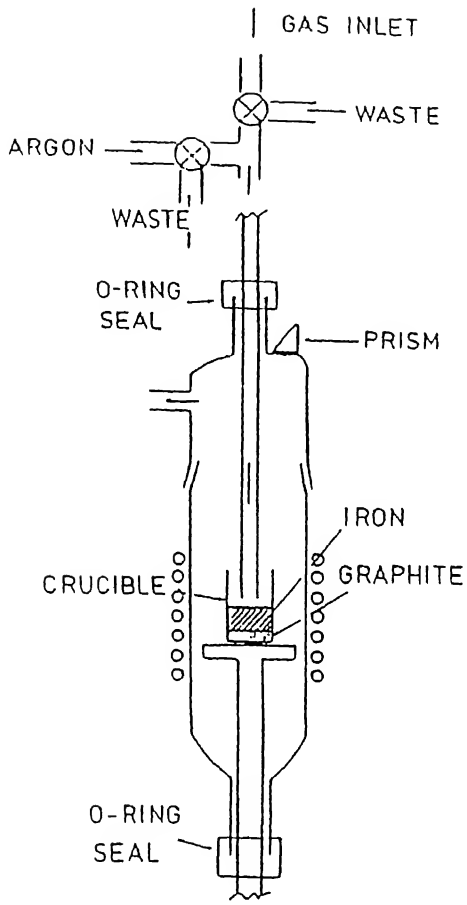

Fig. 1.7 Schematic diagram of experimental arrangement used by Sain and Belton [17].

under the conditions where the rate was not significantly affected by mass transfer in either liquid or gas phases. The value of the rate constant for pure iron was found to be 6.9×10^{-4} mol $cm^{-2}s^{-1}atm^{-1}$ at 1600°C which is almost half of that obtained by Sain and Belton. Addition of small amounts of sulfur to the $Fe\text{-}C_{sat}$ solution lowered the decarburization rate where as the effect of addition of phosphorus and lead on the rate constant was found to be negligible.

The experimental data of above investigation have been used to validate various kinetic models in the present work.

1.2 Emulsion Formation in Steelmaking

Metal droplets are ejected from the jet impact spot in top blown oxygen steelmaking converters. A large fraction of these droplets fall through the surrounding slag-gas mixture while some of them escape through the mouth of the converter or deposit as skull at the mouth of the converter. Simultaneous to the production of metal droplets, gas bubbles, primarily of CO, are produced by decarburization reaction occurring in the jet impingement zone as well as by decarburization reaction at the interfaces of metal droplets and slag, and bulk metal and slag. The falling metal droplets and the rising gas bubbles have finite residence times in slag. The three phase mixture of slag, metal droplets and gas bubbles is referred to in this work as emulsion. The counter current flow of falling metal droplets and rising gas bubbles within the emulsion is of special relevance to slag formation behavior and the kinetics of oxidation/reduction reactions in oxygen steel making converters; for example, excessive gas evolution can result in slopping of the

converter; if a large amount of droplets are retained in the slag then the FeO content of slag is reduced rapidly by the carbon in the droplets and, as a consequence, lime dissolution slows down; on the other hand dissolution of the converter refractory lining may increase with FeO content of slag, etc..

1.2.1 Review of the Previous Work

Turner and Jahanshahi [19] analyzed the emulsification phenomena in top as well as combined blown oxygen steelmaking with the help of a cold model. Mercury and glycerol were used to model the metal and slag phases, respectively. In the top blowing condition, the concentration of metal droplets in the upper phase (slag) was found to increase with lowering of lance while under the conditions of combined blowing maximum metal emulsion formation occurred when the bubblers were located at the bottom right under the impingement zone of the top jet.

Katyama *et al.* [20] studied the influences of a thick layer of slag on smelting reduction. The amount metal droplets in the lower (30 volume%) slag layer reached 30 wt% or more. In the upper region (70 vol% of the slag layer), the concentration of metal droplets depended upon stirring intensity of metal bath for a given slag composition. By employing molybdenum as a tracer, it was observed that 85-95 wt% of the metal droplets had originated from metal bath.

Wei and Oeters [21] investigated the formation of emulsion in injection ladle by carrying out two types of water model experiments: tank with bottom gas injection through tuyers and tank with water jet injection. The number of droplets of slag increased with flow rate of stirring gas but the average diameter of droplets

decreased. The positioning of nozzle at the bottom affected on the number of droplets generated. Emulsion formation was found to be increased when a central nozzle was used.

Standish and He [22-24] investigated the generation of droplets in a laboratory water model by employing top blowing. The variation of droplet generation rate with top gas flow rate is shown in Fig. (1.8) [22]. At low gas flow rates (AB region of Fig. (1.8)), termed as dropping region, a single droplet was seen to gradually form at the crater surface and finally detach from the edge of the crater (see Fig. (1.9)). At high gas flow rates (BC region of Fig. (1.8)), termed as swarming region, along with single droplets, large tears of liquid formed at the edge crater during blowing which finally broke up into several small drops. It was found that bottom blowing significantly increased both the rate of droplet generation and the mean drop size.

The phenomenon of droplet generation, according to He and Standish [23],can be said to be dominated mainly by two factors: first, the momentum intensity of the gas jet at the undisturbed surface of the bath (the momentum intensity is defined as the ratio of jet momentum at a certain distance from the lance nozzle to the corresponding jet cross sectional area); second, the physical properties of liquid from which the droplets are ejected, such as density, viscosity and surface tension. Higher the density, viscosity and surface tension, lower is the droplets generation rate. From the similarity analysis they related the Weber number (which is expressed as a ratio of the momentum intensity to the main liquid properties) of the model to that of the real system. Based on yet another model study of residence time of metal droplets in the slag in BOF

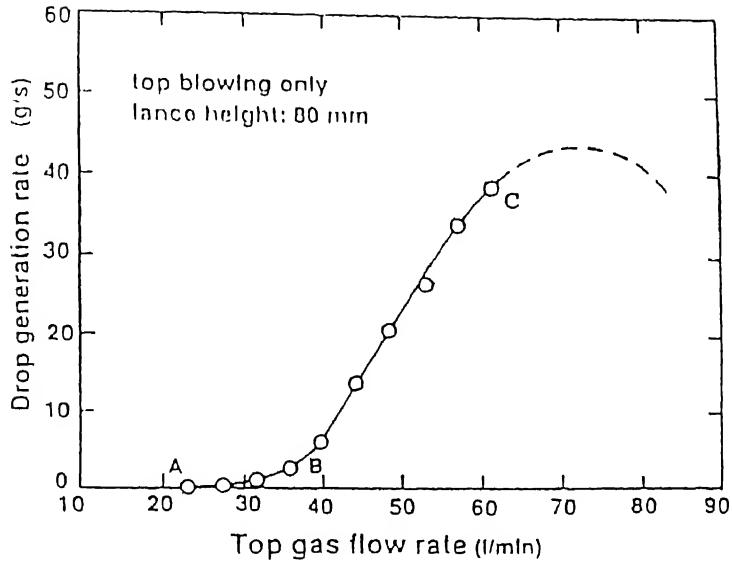

Fig. 1.8 Effect of gas jet momentum on drop generation rate; AB - dropping region, BC - swarming region according to Standish and He [22].

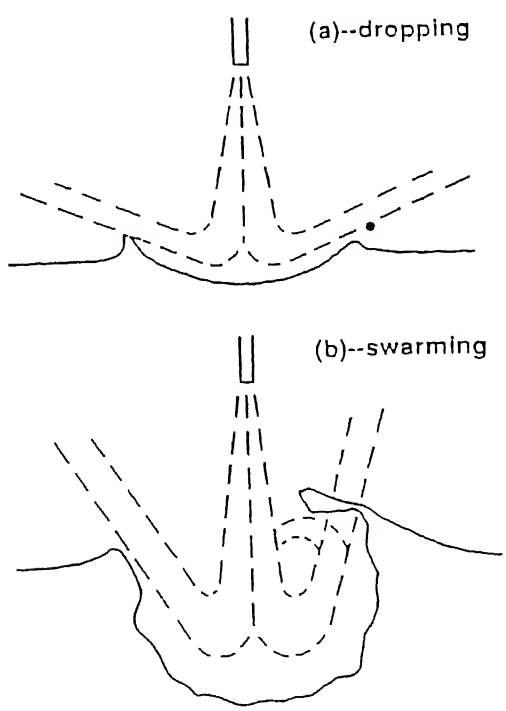

Fig. 1.9 Two different mechanisms of drop generation [22].

steelmaking, He and Standish [24] found that the mean residence time significantly increased with increasing top gas flow rate and decreased with increasing the bottom gas flow rate (in combined blowing); mean residence time was defined as the ratio of the amount of droplets in slag layer and the drop generation rate. The mean residence time first increased and then decreased with lance height.

Gal-OR and Waslo [25] determined the terminal velocity of an ensemble of falling drops (or rising bubbles) in the presence or absence of surfactant. The equations of viscous fluid motion, conservation equation for surfactants and the equation of continuity for both phases were solved by employing a free surface cell model which takes into account hindering effects among neighbor particles. It was found that $U_{ensemble}$ can be expressed in terms of 14 or 15 basic variables, namely

$$U_{ensemble} = f(\rho_c, \rho_d, \mu_c, \mu_d, g, d, \phi, \sigma, \Gamma, \Gamma_o, D_i^s, \alpha^*, D_b^s, \delta) \quad (1.10)$$

$$= f'(\rho_c, \rho_d, \mu_c, \mu_d, g, d, \phi, \Gamma, \Gamma_o, D_i^s, \alpha^*, D_b^s, \delta, \beta_o, T) \quad (1.11)$$

where ρ is density, μ is viscosity, d is diameter of spherical bubble, drop or solid particle, σ is surface tension, Γ is surface concentration of surfactants, Γ_o is equilibrium surface concentration of surfactant concentration of surfactant, ϕ is dispersed phase hold up fraction, D^s is diffusivity of surfactants, δ is thickness of boundary layer of diffusion, α^* overall adsorption rate constant, β_o is constant of adsorption kinetics and the subscripts c, d, i, b denote continuous phase, dispersed phase, interface and bulk phase, respectively. Their analysis showed that $U_{ensemble}$ decreased with retardation coefficient γ. The motion of the ensemble was shown to be

seriously hindered by neighbor particles. $U_{ensemble}$ decreased drastically as the volumetric dispersed phase hold up fraction increased.

From the study of hydrodynamics of gas agitated liquid-liquid dispersions Hatzikiriakos *et al.* [26] concluded that the mean drop size of dispersed phase drops in gas-agitated liquid-liquid dispersions can be expressed as a function of the physical properties of the dispersed phase, bubble boundary layer thickness and energy dissipation rate. According to them, dispersed-phase properties have the greatest impact on mean drop size at low energy dissipation rates whereas boundary layer thickness becomes increasingly important at higher energy dissipation rates.

The mechanism of slag foaming control of smelting reduction process with carbonaceous materials was investigated by Ogawa *et al.* [27] in a 1-ton smelting reduction furnace. In addition X-ray fluoroscopic observations were also made in a small crucible. It was found that the average residence time of CO bubbles depended uniquely on the mass ratio of carbonaceous materials and slag (irrespective of gas volume) and increased with decreasing amount of carbonaceous material in the furnace (Fig. (1.10)). The carbonaceous material is considered to restrain slag foaming by promoting the coalescence of small bubbles on its surface and encourage the bubbles to escape through the top of the slag bath. The slag foaming height decreased with decreasing carbonaceous material size. From the experiment on 100-ton smelting reduction furnace they confirmed that the presence of a certain amount of carbonaceous material in the slag layer was necessary for a stable operation of the smelting reduction furnace.

Ito and Fruehan [28] defined the average gas travelling time

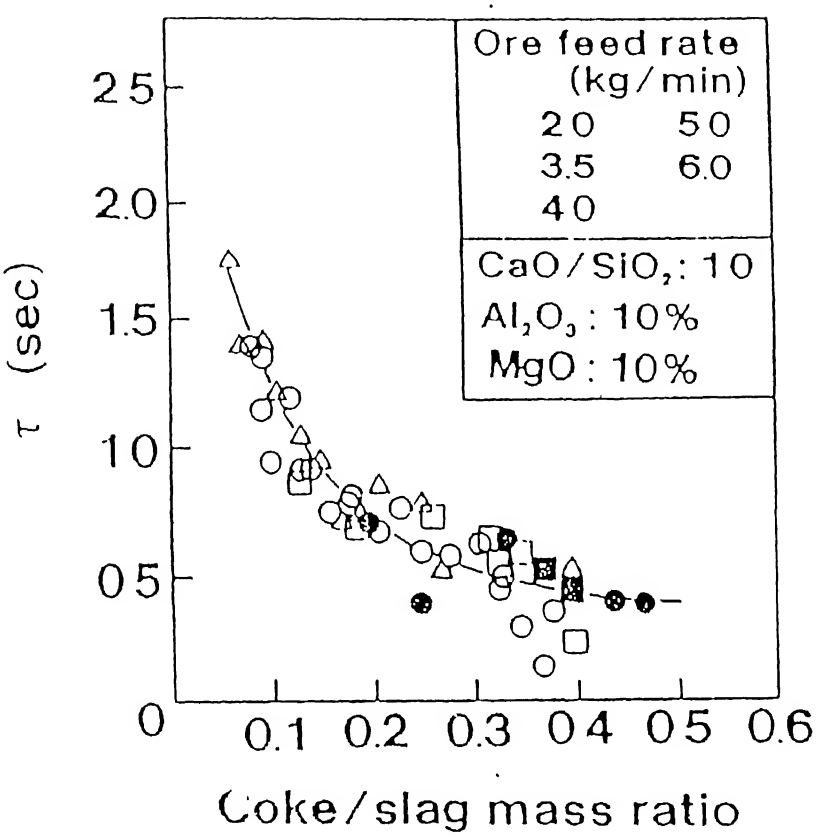

Fig. 1.10 Effect of coke/mass ratio on the average residence time (t) of CO bobbles [27]

as the ratio of change of slag height and superficial gas velocity. The slag foaminess was quantitatively characterized by the average gas traveling time or foaming index (Σ) and average foam life (τ) . It was shown that for an ideal slag where void fraction is independent of foam height $\Sigma = \tau$. In a $CaO-SiO_2-FeO$ system, the foaming index Σ decreased with basicity up to 1.22 at 1400°C; however, when CaO/SiO_2 was greater than 1.22, Σ increased due to presence of second phase particles (CaO or $2CaO\ SiO_2$). Foaming index, Σ, also decreased with increasing temperature because of the decrease of viscosity and the increase in surface tension. From the dimensional analysis [29] they correlated the various slag properties with foaming index as

$$\Sigma = k \frac{\mu}{\sqrt{\sigma\rho}} \qquad (1.12)$$

where k is a dimensional constant, σ is surface tension of slag, ρ is density of slag, μ is viscosity of slag.

The effect of CaF_2 and CaS on the foaming index of a $CaO-Al_2O_3-SiO_2$ ladle type slag at 1500°C was experimentally studied by Roth *et al.* [30]. The foaming index reached a maximum at about 10 wt% CaF_2 in the slag; the addition of FeO shifted the maxima to lower CaF_2 contents. The addition of sulphur did not affect much the foaming behavior of the slag.

Koria and Lange [31] studied the size distribution of molten iron droplets generated by top blowing experiments. It was suggested that droplets followed the Rosin-Rammler-Sperling distribution in terms of limiting diameter of drop, d_{limit}. By using operational data of a particular converter they found that d_{limit} increased with decreasing lance height as the blow progressed.

Ogawa *et al.* [32] proposed a physical model of slag foaming

by using the results of cold and hot model experiments. They confirmed that the size of bubble forming at the slag/metal interface could be determined by the static balance between the buoyancy force and the adhesive force at the slag/metal interface. It was found that besides the surface tension and the viscosity of slag, the slag/metal interfacial tension and the surface tension of metal also affected the foam height . The effects of the properties of slag and metal on bubble size, foam height etc are summarized in Table 1.2.

1.3 Scope of Present Work

In the present work a general kinetic model for reduction of iron oxide in molten slags by iron-carbon melt is developed in Chapter 2. The experimental data reported in the literature are critically analyzed for the first time in the section 2.3,to describe rate governing mechanisms and also determine rate constants (Sec. 2.2). These rate constants can be applied under a variety of conditions encountered in iron and steel production.

A quantitative description of the residence time of metal droplets and gas bubbles in slag-metal-gas emulsion is provided in Chapter 3. A new dimensionless Emulsion number En is proposed in section 3.1. In real oxygen steelmaking converters the reduction rate of FeO in slag by dissolved carbon in ejected metal droplets is correlated with emulsion number (Sec. 3.1). Conclusions are summarized in Chapter 4.

Table 1.2 The effects of the properties of slag and metal on the bubble size at the slag-metal interface, the void fraction of foam, the rupture rate of bubble film and the foam height [32].

	Foam height	Rupture rate of bubble flim	Bubble size	Void fraction of foam
Slag Viscosity ↑	increase	↓	——	↓
Surface tension of slag ↑	decrease	↑	↑	↑
Slag-metal inter-facial tension ↑	decrease	↑	↑	↑
Surface tension of metal ↑	increase	↓	↑	↓

CHAPTER 2

KINETICS OF IRON-OXIDE REDUCTION

2.1 General Kinetic Model

The overall reduction reaction of FeO by Fe-C melt, as discussed in section 1.1,

$$(FeO) + [C] = (Fe) + (CO)_g \qquad (2.1)$$

could be subdivided into gas-slag reaction

$$(FeO) + (CO)_g = (Fe) + (CO_2)_g \qquad (2.2)$$

and gas-metal reaction

$$(CO_2)_g + [C] \rightarrow 2\ (CO)_g \qquad (2.3)$$

The various steps of overall process have been discussed in section 1.1. The relative importance of five steps of reduction of FeO under different experimental conditions can be evaluated as follows. In a carbon-saturated metal the mass transfer of carbon within metal (step 1) can be ignored as rate controlling step [4]. The CO/CO_2 gas bubbles form continuously and grow as a thin film at the interface of gas and metal. If these bubbles detach frequently and reform at the gas-metal interface, as observed experimentally, then mass transport of CO and CO_2 in the gas phase can also be neglected as a rate controlling step. However, at low concentrations of iron oxide in slag the mass transfer of FeO in slag can become one of the rate controlling steps (i.e., step 4). Only at higher concentrations of FeO in slag, when oxide ions are present in slag in sufficient quantity to facilitate ionic conduction, the mass transfer of FeO in slag can be ignored as a rate controlling step and then

gas-slag chemical reaction itself (step 5) can become a rate controlling step. In both cases (i.e., at low and high FeO concentrations) gas-metal chemical reaction (step 2) could act as one of the active rate controlling steps. The gas-metal reaction can be subdivided into dissociative chemisorption of CO_2 and chemical reaction of adsorbed oxygen with dissolved carbon

$$(CO_2)_g \rightarrow (CO)_g + [O]_{ad} \qquad (2.3a)$$

$$[O]_{ad} + [C] \rightarrow (CO)_g \qquad (2.3b)$$

Dissociative chemisorption of CO_2 (Eq. 2.3a) has been shown to be a slow process [3,17] at iron and steelmaking temperatures (due to a very small value of CO_2/CO ratio at high carbon content of melt). Owing to scarcity of CO_2 at gas-metal interface the reaction (2.3a) can slow down to such an extent that it becomes rate controlling [3]. At intermediate FeO concentrations, all the three steps (steps 2,4 and 5) can control the overall reaction (given by Eq. 2.1).

The overall rate equation for the reduction of FeO in slag-gas-metal system (considering steps 2, 4 and 5 as rate controlling) can be derived as follows :

The rate equation for reaction (2.2) can be written as

$$-\frac{d(n_{CO})}{dt}\bigg|_{gas\text{-}slag} = A.k_2\left[a^{i}_{FeO}p_{CO} - \frac{a_{Fe}\,p_{CO2}}{K}\right] \qquad (2.4)$$

where a_{Fe} is the activity of iron(=1), a^{i}_{FeO} is the activity of FeO at gas-slag interface, A is the gas-metal and gas-slag reaction area, k_2 is rate constant of forward reaction, K is the equilibrium constant of reaction (2.2), and p_{CO2} and p_{CO} are partial pressure of CO_2 and CO gas, respectively.

The rate equation for reaction (2.3a) is given by

$$-\frac{d(n_{CO2})}{dt}\Bigg|_{gas\text{-}metal} = A\, k_{3a}\, p_{CO2} \qquad (2.5)$$

where k_{3a} is the reaction rate constant of reaction (2.3a). It should be noted that reaction (2.3a) is considered to be an irreversible reaction because as soon as CO_2 dissociates in to CO and O_{ad}, the latter reacts with dissolved carbon.

The mass transfer rate of FeO in slag is given by

$$-\frac{d(n_{FeO})}{dt}\Bigg|_{from\ bulk} = A\, k_{FeO}\left[C^{b}_{FeO} - C^{i}_{FeO} \right] \qquad (2.6)$$

where k_{FeO} is the mass transfer coefficient of FeO in slag and C^{b}_{FeO} and C^{i}_{FeO} are the concentration of FeO in the bulk of the slag and at slag-gas interface, respectively.

From reaction (2.2)

$$-\frac{d(n_{CO})}{dt}\Bigg|_{gas\text{-}slag} = \frac{d(n_{CO2})}{dt}\Bigg|_{gas\text{-}slag} \qquad (2.7)$$

and under steady state conditions,

$$\frac{d(n_{CO2})}{dt}\Bigg|_{gas\text{-}slag} = -\frac{d(n_{CO2})}{dt}\Bigg|_{gas\text{-}metal} \qquad (2.8)$$

Thus, from Eq. (2.7) and (2.8)

$$-\frac{d(n_{CO})}{dt}\Bigg|_{gas\text{-}slag} = -\frac{d(n_{CO2})}{dt}\Bigg|_{gas\text{-}metal} \qquad (2.9)$$

and from Eqns (2.4), (2.5) and (2.9)

$$A.k_2\left[a^{i}_{FeO}\, p_{CO} - \frac{a_{Fe}\, p_{CO2}}{K} \right] = A\, k_{3a}\, p_{CO2} \qquad (2.10)$$

$$\text{therefore,}\quad p_{CO2} = \frac{a^{i}_{FeO}\, k_2\, p_{CO}}{\left[k_{3a} + \frac{k_2}{K} \right]} \qquad (2.11)$$

Substituting p_{CO2} value in Eq.(2.4)

$$-\frac{d(n_{CO})}{dt}\Bigg|_{gas\text{-}slag} = a^{i}_{FeO}\, p_{CO}\, A \left[\frac{1.0}{\frac{1}{k_2} + \frac{1}{K.k_{3a}}}\right] \tag{2.12}$$

Now from reaction (2.2)

$$-\frac{d(n_{CO})}{dt}\Bigg|_{gas\text{-}slag} = -\frac{d(n_{FeO})}{dt}\Bigg|_{gas\text{-}slag} \tag{2.13}$$

and from mass conservation of FeO

$$-\frac{d(n_{FeO})}{dt}\Bigg|_{gas\text{-}slag} = -\frac{d(n_{FeO})}{dt}\Bigg|_{from\ bulk} \tag{2.14}$$

Thus from Eq. (2.13) and (2.14)

$$-\frac{d(n_{FeO})}{dt}\Bigg|_{from\ bulk} = -\frac{d(n_{CO})}{dt}\Bigg|_{gas\text{-}slag} \tag{2.15}$$

From eqns (2.6), (2.12) and (2.15)

$$A\, k_{FeO}\left[C^{b}_{FeO} - C^{i}_{FeO}\right] = a^{i}_{FeO}\, p_{CO}\, A \left[\frac{1.0}{\frac{1}{k_2} + \frac{1}{K.k_{3a}}}\right] \tag{2.16}$$

since $$C^{i}_{FeO} = \frac{a^{i}_{FeO}\, n_{tot}}{Vl_s\, \gamma_{FeO}}$$

$$a^{i}_{FeO} = \frac{k_{FeO}\, \gamma_{FeO}\, Vl_s\, C^{b}_{FeO}\, (k_2 + K k_{3a})}{k_{FeO}\, n_{tot}\, (k_2 + K k_{3a}) + p_{CO}\, K\, k_2\, k_{3a}\, \gamma_{FeO}\, Vl_s} \tag{2.17}$$

where Vl_s is the volume of the slag, n_{tot} is the total number of mole of slag and γ_{FeO} is the activity coefficient of FeO in slag.

Substituting a^{i}_{FeO} into Eq. (2.12) and from Eq. (2.15)

$$-\frac{d(n_{FeO})}{dt}\Bigg|_{from\ bulk} = A\, C^{b}_{FeO} \left[\frac{1.0}{\frac{1}{\alpha.k_2} + \frac{1}{\alpha.K.k_{3a}} + \frac{1}{k_{FeO}}}\right] \tag{2.18}$$

where $\alpha = \frac{p_{CO}\ \gamma_{FeO}\ Vl_s}{n_{tot}}$

On integrating Eq.(2.18) the final expression for rate equation is given by

$$- \ln \left\{\frac{FeO_t}{FeO_o}\right\} = \frac{A.t}{Vl_s} \left[\frac{1.0}{\frac{1}{\alpha.k_2} + \frac{1}{\alpha.K.k_{3a}} + \frac{1}{k_{FeO}}}\right] \qquad (2.19)$$

where FeO_o and FeO_t are the concentration of FeO in slag at initial time and at time t, respectively, in wt%.

Three different kinetic models can now be considered.

Model-I: For low concentration of FeO (< 5 wt%) when dissociative chemisorption of CO_2 at gas-metal interface and mass transfer of FeO in slag become rate controlling. For this case Eq. (2.19) reduces to

$$-\ln \left\{\frac{FeO_t}{FeO_o}\right\} = \frac{A.t}{Vl_s} \left[\frac{1.0}{\frac{1}{\alpha.K.k_{3a}} + \frac{1}{k_{FeO}}}\right] \qquad (2.20)$$

Model-II: For intermediate concentration of FeO (5-40 wt%) in slag when all three steps (Steps 2, 4, 5) become rate controlling. The overall rate equation is same as Eq. (2.19)

Model-III: For high FeO concentration (> 40 wt% FeO in slag) when dissociative chemisorption of CO_2 and gas-slag reaction become rate controlling. In this case Eq. (19) reduces to

$$- \ln \left\{\frac{FeO_t}{FeO_o}\right\} = \frac{A.t}{Vl_s} \left[\frac{1.0}{\frac{1}{\alpha.k_2} + \frac{1}{\alpha.K.k_{3a}}}\right] \qquad (2.21)$$

It will be shown later that the limits 5 wt% FeO (for Model-I) and 40 wt% FeO (for Models-III) actually correspond to switch over points around which the governing mechanisms change from one set of rate controlling steps to another.

2.2 Estimation of Rate Constants and Activity Coefficient of FeO

In order to predict the variation of iron oxide (FeO) content of a given slag with time with help of kinetic models the values of reaction rate constants (k_2 and k_{3a}) and the activity coefficient of FeO in slag (γ_{FeO}) are needed apriori.

2.2.1 Gas-Metal Reaction

Sain and Belton [17] studied the gas-metal reaction in the temperature range 1160-1600°C and reported the dependence of rate constant on temperature as

$$k_{3a} = 9.87 \times 10^3 \times \exp\left(\frac{-11,700}{T} - 0.48\right) \qquad (2.22)$$

where k_{3a} is in mol $m^{-2}s^{-1}bar^{-1}$.

At 1600°C Mannion and Fruehan [18] reported k_{3a}= 6.81 mol $m^{-2}s^{-1}bar^{-1}$ where as according to Cramb and Belton [33] k_{3a}= 7.79 mol $m^{-2}s^{-1}bar.^{-1}$ These values of k_{3a} are approximately half the k_{3a} value calculated from Eq.(2.22) (which is 11.84 mol $m^{-2}s^{-1}bar^{-1}$ at 1600°C). According to Mannion and Fruehan, rate of decarburization was overestimated in the experiments of Sain and Belton due to the use of batch weight loss technique. In the present work Eq.(2.22) is, however, retained due to two reasons

- at lower temperatures when decarburization rate is slower, the error due to batch weight loss technique would be much smaller.
- Eq.(2.22) provides k_{3a} values over a range of temperature where as other investigators have calculated the k_{3a} value only at one temperature (1600°C).

2.2.2 Gas-Slag Reaction

Sato *et al.* [7] studied the reduction of pure iron oxide

melt by solid carbon and also by carbon dissolved in molten iron. Results of their experiments (as shown in Fig. (1.3)) can be used to evaluate the rate constant (k_2) for gas-slag reaction. In the case of pure iron oxide melt the mass transfer of FeO in slag may not be rate controlling due to the presence of sufficient quantity of oxide ions (O^{2-}) in the slag. Model-III (i.e, Eq. 2.21) can thus be used to evaluate k_2. The k_2 values calculated in this work by using experimental data of Sato *et al.* [7] are plotted in Fig. (2.1) as a function of temperature (1420-1620°C) and they can be represented by

$$\ln k_2 = - \frac{32,345.4(\pm 6,128)}{T} + 19.0(\pm 3.42) \qquad (2.23)$$

with standard deviation, $\sigma_{\ln k_2, 1/T} = \pm 0.3$

Nagasaka *et al.* [14] and Fine *et al.* [15] studied the reduction of iron oxide slag by CO gas. The k_2 values obtained from their experimental data are lower than that calculated by Eq. (2.23), as given below:

k_2= 0.11 mol $m^{-2}s^{-1}bar^{-1}$, with pure iron oxide melt, according to Nagasaka *et al.* [14] where as from Eq. (2.23) k_2= 0.72 mol $m^{-2}s^{-1}bar^{-1}$ at 1400°C.

k_2= 0.31 mol $m^{-2}s^{-1}bar^{-1}$, with 67.7% FeO in slag, according to Fine *et al.* [15] where as from Eq.(2.23) k_2= 5.64 mol $m^{-2}s^{-1}bar^{-1}$, at 1600°C

The above differences in k_2 values may be attributed, primarily, to the difference in experimental conditions. For example, in the work of Nagasaka *et al.* and Fine *et al.* CO gas was passed over the slag layer and thus there was no mixing of bulk slag due to CO gas evolution. This could have slowed down the reaction rate thereby giving rise to lower k_2 values. In contrast, in the work of Sato *et al.* [7] CO bubbles formed in between slag and metal and on detachment they rose through slag as most often the case in several experiments

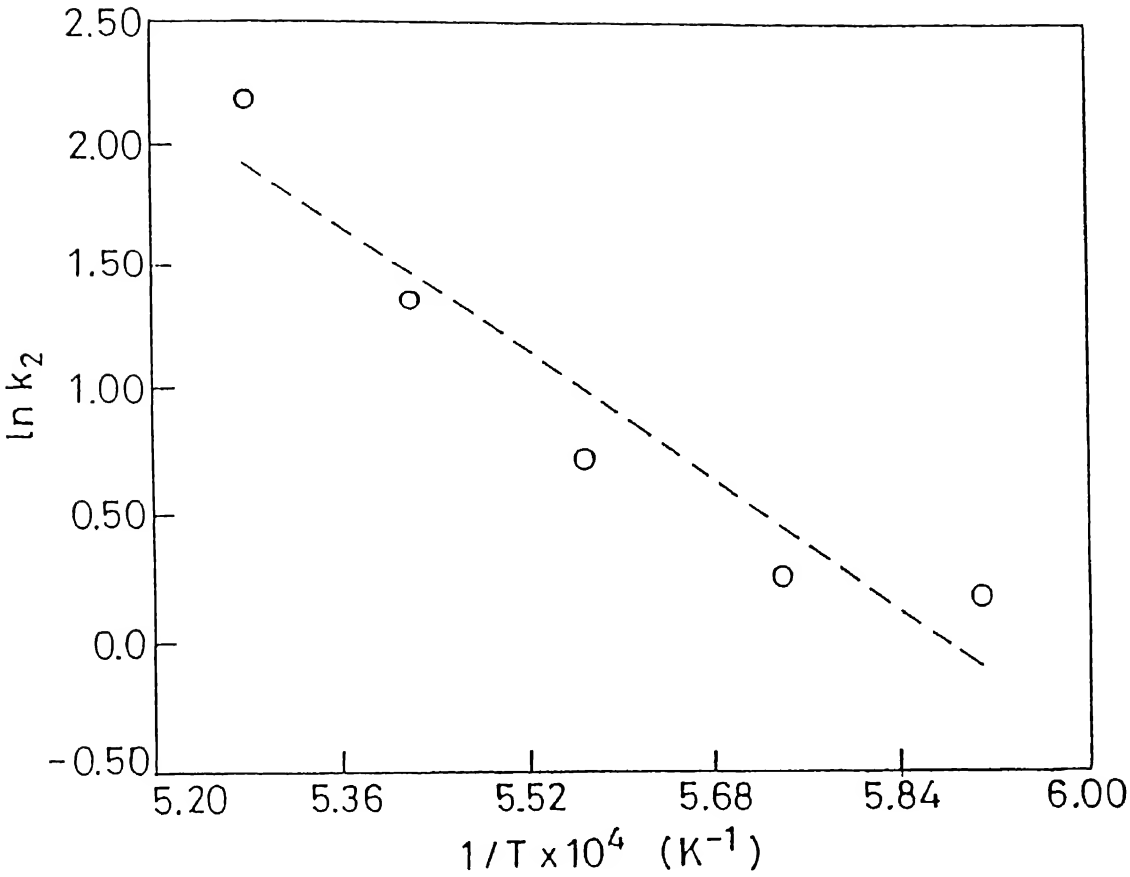

Fig. 2.1 Variation of rate constant (k_2) with temperature; open circles refer to calculated values of $\ln k_2$ using experimental data from ref. [7].

reported in literature.

2.2.3 Activity Coefficient of FeO in Slag

Activity coefficient of FeO in slag (γ_{FeO}) is required in Eqns (2.19), (2.20) and (2.21) so as to compute the value of k_{FeO}. In the present work the Regular Solution model [34] has been used to estimate γ_{FeO} in $CaO-FeO-Al_2O_3-SiO_2$ slags. (Regular solution model as well as a sample calculation are given in Appendix-A).

The equilibrium constant (K) for reaction (2.2), appearing in Eqns (2.19), (2.20) and (2.21), is calculated from [35]

$$\Delta G^{\circ} = -49,705 + 47.50T \text{ (J)} \qquad (2.24)$$

2.3 Application of Models I,II,III to Slag-Gas-Metal System

A careful study of the investigations reported in the literature has shown in the present work that slags can be divided into three classes : slags containing 5 wt% FeO or less, slags containing 5-40 wt% FeO and, finally, slags containing more than 40 wt% FeO.

2.3.1 Slags Containing Low FeO (less than 5 wt% FeO)

The review of the previous work (Sec. 1.1.1) shows that Sommerville *et al.* [3] and Hasham *et al.* [4] investigated the FeO reduction for low FeO slag (less than or around 5 wt% FeO). Their experimental data, as shown in Fig. (1.1) and (1.2) as well as given in Table 1.1, were used to calculate the mass transfer coefficient of FeO in slag phase according to Model-I (Eq. 2.20) (sample calculation is given in Appendix-B) and the values of k_{FeO} obtained in this way are given Table 2.1. Various values of the mass transfer coefficient

of FeO in slag have been reported by other investigators: Bafghi *et al.* [11] $k_{FeO} \simeq 6.0 \times 10^{-5}$ m/s and Wei *et al.* [10] $k_{FeO} \simeq 3.0 \times 10^{-5}$ m/s. The comparison shows an agreement between calculated values of k_{FeO} (Table 2.1) with reported values. The values reported by Bafghi *et al.*[8]) are slightly higher than the values given in Table 2.1 (this may be due to the turbulent conditions prevailing in their experiment - stirring speed of 100 rpm. of slag phase). The variation of concentration of FeO in slag with time have been plotted in Fig. (2.2a) and the close agreement between model predicted curve and experimental data shows the confirmation of Model-I (i.e., the reduction process is controlled both by chemical reaction at gas-metal interface and mass transfer of FeO in slag) for a slag containing less than 5 wt% FeO.

2.3.2 Slags Containing 5-40 wt% FeO

The experimental results of Sato *et al.*[8] for the reduction of FeO (5-50 wt%) in $CaO-Al_2O_3-SiO_2$ slags are shown in Fig. (1.5). Analysis of their experimental data during first ten minutes reveals that with gradual increase in FeO content of slag the reaction mechanism changes from mixed control (which is mass transfer of FeO in slag + chemical reaction at gas-metal interface, Model-I, Eq.20) to mixed chemical reaction control (which is chemical reaction at gas-slag and chemical reaction at gas-metal interfaces, Model-III, Eq. 21) via an intermediate stage (~ 5-40 wt% FeO) where all the three steps (mass transfer of FeO in slag + chemical reaction at gas-metal and chemical reaction at gas-slag interfaces, Model-II, Eq.2.19) are rate controlling. Fig. (2.2a) and (2.2b) compare the results of model prediction and the experimental results of Sato *et al.* [8] The calculated values of k_{FeO} (as discussed in Appendix B) are given in

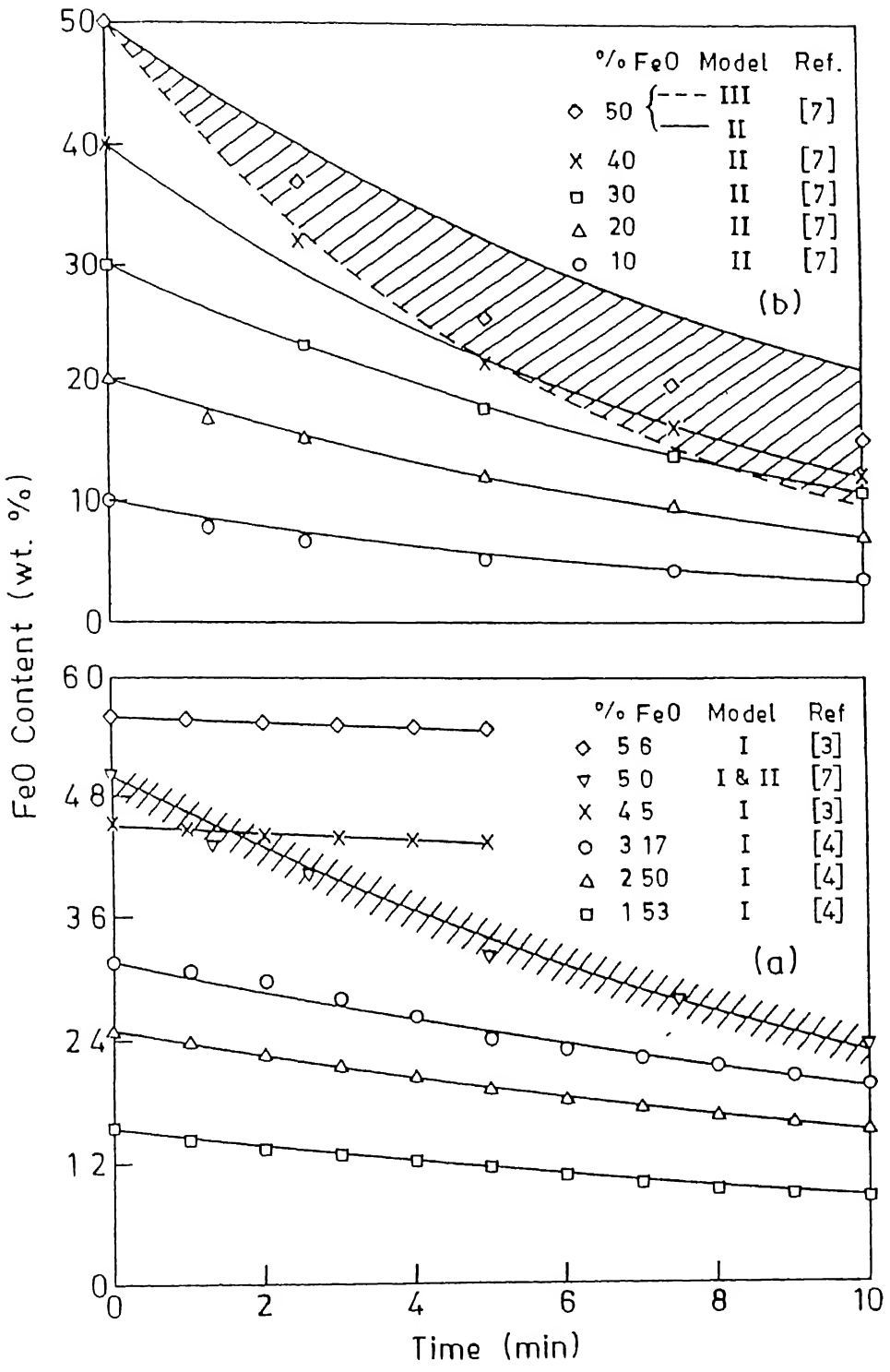

Fig. 2.2 Variation of FeO content (wt%) for different slags with time; all lines correspond to model calculations as indicated. Hatched region in (a) shows transition zone from Model-I to Model-II and hatched region in (b) shows transition zone from Model-II to Model-III.

Table 2.1. The experimental data for slags containing approximately 5 wt% FeO, can be interpreted by both Model-I and Model-II (Table 2.1). The hatched region in Fig (2.2a) shows that change over from mixed control (Model-I) to intermediate mode (Model-II) takes place around 5 wt% FeO in slag.

2.3.2 Slags Containing High FeO (more than 40 wt% FeO)

The experimental data points of Sato *et al.* [8] for slags containing 50 wt% FeO lie in between the lines corresponding to Model-II (assuming $k_{FeO} = 4.0 \times 10^{-5}$ m/s) and Model-III (see hatched region in Fig. 2.2b).

The above classification of kinetic models based FeO content of slag will become clearer if the resistance offered by each step is calculated separately from Eq. (2.19), as follows:

-Resistance due to mass transfer of FeO in slag, $M = \frac{1}{k_{FeO}}$ (2.25a)

-Resistance due to gas-slag chemical reaction, $Rs = \frac{1}{\alpha . k_2}$ (2.25b)

-Resistance due to gas-metal chemical reaction, $Rm = \frac{1}{\alpha . K . k_{3a}}$ (2.25c)

The relative resistance due to mass transfer of FeO alone can be calculated from

$$M' = [M/(M+Rs+Rm)] \times 100 \quad (2.26)$$

Similarly, relative resistance arising due to other two rate controlling steps can also be calculated.

Actual resistances and relative resistances are calculated according to Eqns (2.25) and (2.26) (for the data obtained from Sato at el. [8]) and are plotted against FeO content of slag, in Fig. (2.3). For the sake of a uniformity in experimental conditions only the work of Sato at el. is considered. According to Fig. (2.3a), when the Feo content of slag increases, the actual resistance due to mass

transfer decreases. The individual resistance offered by two chemical reaction rate controlling steps, namely, gas-slag reaction and gas-metal reaction, remain more or less constant at a temperature (1520°C). This is to be expected. The magnitudes of relative resistances (Fig. 2.3(b)) reveal that at lower FeO contents (<5 wt%) mass transfer dominates the reduction process (i.e, it is predominantly mass transfer controlled). However, at FeO content greater than 50 wt%, the extrapolation of curves show that the contribution of mass transfer resistance decreases rapidly. It may be due to two reasons: the mass transfer coefficient of an ionic constituent like FeO increases with concentration; also CO gas generation rate increases with amount FeO and this results in higher turbulence of slag phase. One can safely conclude that the change over from Model-II to Model-III may take place between 50-60 wt% FeO (depending upon experimental conditions). Beyond 60 wt% FeO chemical reactions at gas-metal interface and gas-slag interface will be rate controlling (Model-III). Elaborate experiments are, however, required in the range 40 to 65 wt% FeO to find out the change over point from Model-II to Model-III more precisely. It is important to note here that in all the cases actual resistance as well as the relative resistance due to gas-metal reaction are greater than that offered gas-slag reaction (Fig. (2.3)). Some investigators [3] concluded that the process is controlled by gas-metal reaction only. They ignored the resistance offered by gas-slag reaction, both the resistances need to be considered (Fig. (2.3)).

As discussed in Sec. 1.1.1, Wei *et al.* [9] used a slightly different experimental arrangement (with a stirrer at 200 rpm). At such high stirring speeds the mass transfer of FeO in slag may not be rate controlling and thus the process becomes mixed chemical reaction

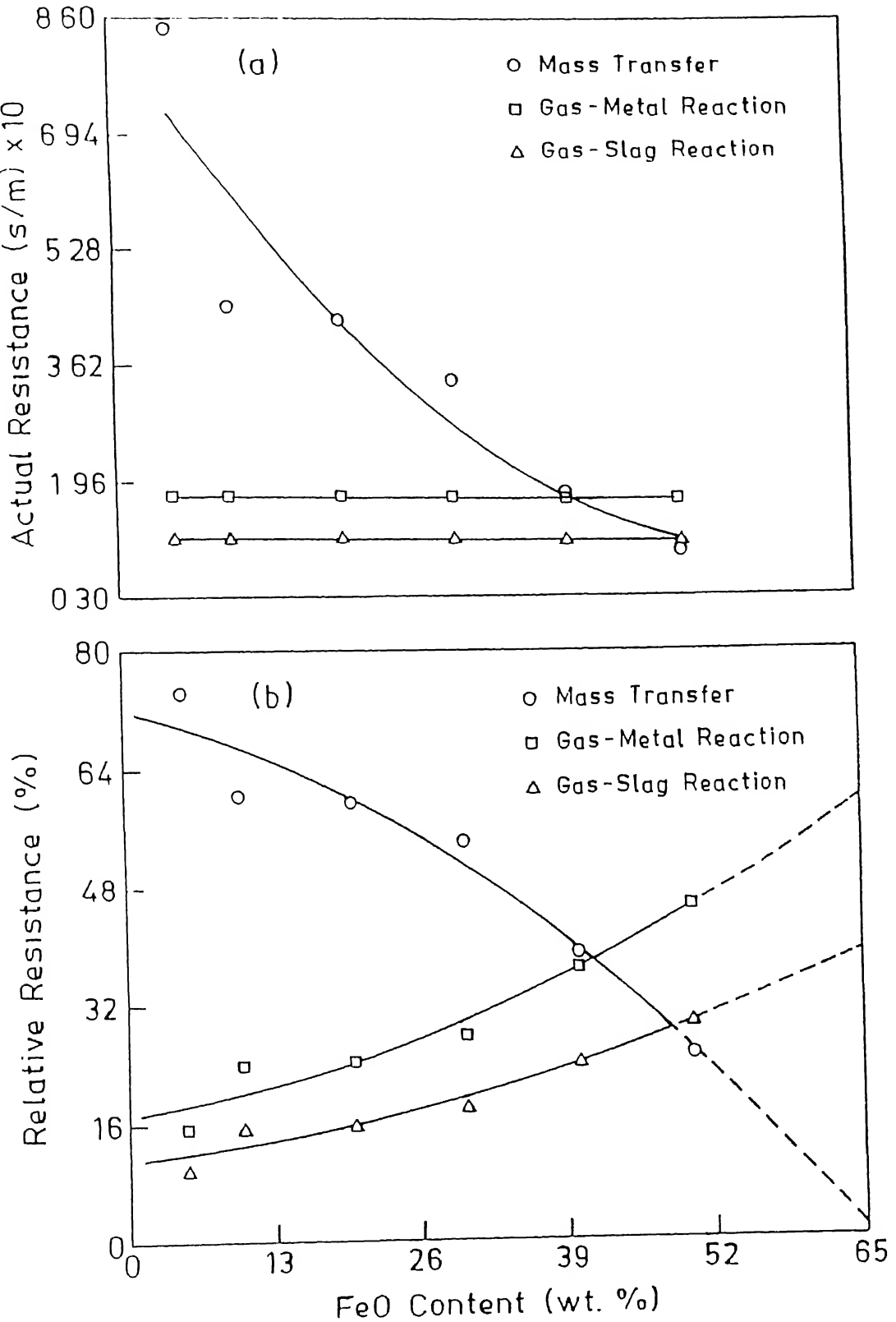

Fig. 2.3 Resistances offered by various rate controlling steps at different FeO content of slags: (a) Actual resistances vs. FeO content (b) Relative resistances vs. FeO content; dotted lines are extrapolated.

controlled (i.e, chemical reaction at gas-metal interface and chemical reaction at gas-slag interfaces, Model-III), even below 40% FeO. Near agreement between k_2 values, obtained from Eq. (2.23) and from the analysis of experimental data of Wei *et al.* (Fig. (1.6)) for 10, 15 and 20% FeO slag at 200 rpm. is evident from Table 2.1 (written inside brackets); small differences in the rate constant values can be partly attributed to the differences in slag compositions employed in the experiments. For example, in most experiments $CaO-Al_2O_3-SiO_2$ master slag was used where as Wei et.al. used $CaO-FeO-Li_2O-SiO_2$ slag.

Some of the reported experimental data [3, 36-37] could not be analyzed in this work due to complex and/or non-reproducible experimental conditions. For example, Tarby and Philbrook [36] reduced FeO in slag by Fe-C melt in a graphite crucible. They concluded that the process was mass transfer controlled. In their experiment, however, it is difficult to separate the amount of FeO reduced by Fe-C melt and by the graphite crucible itself. Similarly, Hasham *et al.* [4] investigated the reduction of FeO in slag droplets floating on the surface of the Fe-C melt. In such an experiment it is difficult to determine the actual interfacial area of reaction since the liquid slag droplets flatten out partially on liquid metal surface and reduce in size as FeO reduction proceeds with time. Borgianni [37] carried out FeO reduction by coke particles; the interfacial reaction area in this case is also not well defined.

Table 2.1 Rate constant values estimated for different experiment conditions.

Ref.	FeO content (wt%)	Temp. (°C)	Rate* controlling steps	# k_{3a}	▌ k_2	$k_{FeO} \times 10^5$ (m/s)
Sommerville *et al.*[3]	1.53	1390	Model-I	5.37	-	2.40
	2.50	1380	,,	5.15	-	2.20
	3.17	1380	,,	5.15	-	2.07
Hasham *et al.*[4]						
1drop.	5.60	1450	,,	6.86	-	2.95
5drops	4.50	1450	,,	6.86	-	3.06
Sato *et al.*[8]	5.0	1520	,,	8.95	-	1.04
	5.0	1520	Model-II	8.95	2.62	1.18
	10.0	1520	,,	8.95	2.62	2.25
	20.0	1520	,,	8.95	2.62	2.35
	30.0	1520	,,	8.95	2.62	2.94
	40.0	1520	,,	8.95	2.62	5.57
	50.0	1520	,,	8.95	2.62	10.63
	50.0	1520	Model-III	8.95	2.62 (1.41)	-
Wei$ *et al.*[9]	10.0	1300	,,	3.59	0.21 (0.29)	-
	15.0	1300	,,	3.59	0.21 (0.30)	-
	20.0	1300	,,	3.59	0.21 (0.31)	-
Sato *et al.*[7]	100.0	1600	,,	11.84	5.64	-

k_{3a} values are calculated from Eq.(2.22) and its unit is mol m^{-2} s^{-1} bar^{-1}

▌ k_2 values are calculated from Eq.(2.23) and its unit is $molm^{-2}s^{-1}bar^{-1}$; values in brackets are obtained from experimental data

* Model-I, Model-II and Model-III are according to text (i.e, Model-II or Model-III)

. Metal droplets dispersed in slag.

$ Slag phase stirred at 200 rpm.

CHAPTER 3

STUDY OF SLAG-GAS-METAL DROPLETS EMULSION IN STEELMAKING

3.1 Theoretical Considerations

At the outset, it is convenient to define a dimensionless Emulsion number, En, as follows:

$$En = \frac{\text{Mean residence time of metal droplets in slag, } t_{avg}}{\text{Mean residence time of gas bubbles in slag, } t_g} \tag{3.1}$$

For a given physical system with an emulsion height of h, Eq. (3.1) can be rewritten as

$$En = \frac{t_{avg}}{t_g} = \frac{\langle h/V_d \rangle}{\langle h/V_g \rangle} \tag{3.2}$$

where V_d is the settling velocity of droplets, V_g is the rising velocity of gas bubbles in the gas-slag mixture; symbol <> denotes the mean value of the expression within.

As discussed in Sec. 1.2.1, Gal-Or and Waslo [25] studied the hydrodynamics of an ensemble of drops and bubbles and proposed an expression for the terminal velocity (of droplets or bubbles)

$$U_{ensmeble} = \frac{2}{9} \cdot \frac{\left(\rho_d - \rho_c \right) g\, d^2}{\mu_c} \cdot \Delta \tag{3.3}$$

where $$\Delta = \frac{3\mu_c\left(1-\phi^{1/3}\right)\left(1-\phi^{5/3}\right) + \left[3-\frac{9}{2}\left(\phi^{1/3}-\phi^{5/3}\right)-3\phi^2\right]\left(\mu_d+r\right)}{2\mu_c\left(1-\phi^{5/3}\right) + \left(3+2\phi^{5/3}\right)\left(\mu_d+r\right)}$$

and r is the retardation coefficient due to presence of surfactants

(by definition, $r = -\frac{1}{3}\zeta \frac{\partial\sigma}{\partial\Gamma}$), ϕ is the dispersed phase hold up fraction, ρ is the density, μ is the viscosity d is the radius of liquid droplets (or of gas bubbles), ζ is the retardation constant, σ is the surface tension and Γ surface concentration of surfactants; subscripts c and d stand for continuum and dispersed phases, respectively.

In a slag-metal droplet-gas bubble emulsion the metal droplets may be assumed to fall through gas-slag continuum where as the gas bubbles may be assumed to rise through the continuum of slag and metal. If it is assumed that surfactant concentration does not vary much and also the surface tension of slag varies little with surfactant concentration, then $r \simeq 0$ [25]. The expression for droplet velocity from Eq. (3.3) can now be written as

$$V_d = \frac{1}{18} \frac{\left(\rho_m - \rho_{sg}\right) g\, d_m^2}{\mu_{sg}} \Delta_{sm} \tag{3.4}$$

where $$\Delta_{sm} = \frac{3\mu_{sg}\left(1-\phi_m^{1/3}\right)\left(1-\phi_m^{5/3}\right) + \left[3-\frac{9}{2}\left(\phi_m^{1/3}-\phi_m^{5/3}\right)-3\phi_m^2\right]\mu_m}{2\mu_{sg}\left(1-\phi_m^{5/3}\right) + \left(3+2\phi_m^{5/3}\right)\mu_m}$$

and d_m is the metal droplet diameter; subscripts m and sg stand for metal and slag-gas continuum, respectively. If the volume fraction of dispersed metal phase is very small then the interaction between droplets (coalescence, collision etc.) can be neglected by assuming $\Delta_{sm} = 1$. Similar to the velocity of metal droplets, the expression for the rising velocity of gas bubbles, V_g, can be obtained from Eq. (3.3); with the approximations $\mu_g << \mu_{sm}$ and $r \simeq 0$.

$$V_g = \frac{1}{12} \frac{\left(\rho_{sm} - \rho_g\right) g\, d_b^2}{\mu_{sm}} \left(1-\phi_g^{1/3}\right) \tag{3.5}$$

where d_b is the gas bubble diameter and the subscripts g and sm stand for metal slag-metal continuum. It is clear that in order to evaluate V_d and V_g the values of d_m, d_b, ϕ_m, ϕ_g, μ_{sg}, μ_{sm}, ρ_{sg} and ρ_{sm} will be needed.

Koria and Lange [31] have introduced the concept of upper limiting size, d_{llm}, for the spectrum of droplets produced by impinging gas jet (Sec. 1.2.1). The method of calculation of size distribution of droplets as well as the change in d_{llm} as a function of process variables (like nozzle design, supply pressure of oxygen etc.) are explained in Appendix C. The average size of metal droplet d_{avg} can be expressed in terms of maximum size of droplet, d_{llm} (see Appendix C)

$$d_{avg} = 0.2\ d_{llm} \tag{3.6}$$

where $d_{llm} = 5.513\text{x}10^{-6} \left\{ 10^6 \left(\frac{d_t}{x} \right)^2 p_a \left[1.27 \left(\frac{p_o}{p_a} \right) - 1 \right] \cos\theta \right\}^{1.206}$

Size of a gas bubble increases as it rises through the liquid. The maximum size of the bubble is determined by the balance of forces including surface tension, static pressure, buoyancy force etc. After expanding to certain size gas bubbles may disintegrate into smaller bubbles. No detailed investigations have been reported in literature to estimate the size of bubbles in steelmaking slags. As a first approximation, the critical diameter for disintegration of a gas bubble, d_{bcr}, can be estimated [38] from

$$d_{bcr} = \left[2 \left(\frac{6}{\xi} \right)^{1/3} \frac{\sigma_s}{0.52\ g \left(\rho_g\ \rho_{sm}^2 \right)^{1/3}} \right]^{1/2} \tag{3.7}$$

where σ_s is the surface tension of slag and ξ is the friction factor

[38]. For the sake of simplicity, in this work it is assumed that gas bubbles follow normal size distribution hence the average size of gas bubbles is $d_{bcr}/2$.

Gas fraction, ϕ_g, can be estimated from initial slag volume, foam height and the effective volume of slag phase (i.e, volume obtained after subtracting the volume of the cone of impinging jet(s) submerged in emulsion). Ito and Fruehan [28] have reported that ϕ_g varies between 0.7 to 0.9. The fraction of metal droplets in emulsion mainly depends on amount metal droplets ejected per unit time from bath (defined as iron conversion, Mg, kg/s) and also on the residence time of droplets in the emulsion. He and Standish [23] have proposed a functional relationship between iron conversion, Mg, and Weber number (We)

$$Mg = f(We) \tag{3.8}$$

The Weber number is defined [23] as

$$We = \frac{\rho_g \, u_{o,x}^2}{\left(\rho_m \, g \, \sigma_m\right)^{1/2}} \tag{3.9}$$

where $u_{o,x}$ is center line velocity of gas jet at distance x from the nozzle exit and σ_m is the surface tension of metal. Center line velocity of the jet depends upon nozzle design, lance height and process parameters (such as supply pressure of oxygen). The ratio of dynamic pressure of gas jet at nozzle exit and at any lance height, x, [38] is given by

$$\frac{\rho_x \, u_{o,x}^2}{\rho_e \, u_e^2} = \frac{1}{4}\left(\frac{d_e}{x}\right)^2 \frac{1}{\beta} \tag{3.10}$$

where d_e is exit diameter of nozzle, ρ_e is density of jet at nozzle exit, ρ_x is density of jet at lance height, x, u_e is velocity of gas

at nozzle exit and β is the nozzle constant; in this work $\beta = 6.6 \times 10^{-3}$ has been assumed [38].

From nozzle theory, the velocity of gas at nozzle exit, u_e, is given by [38]

$$u_e = \left\{ \left(\frac{2\gamma}{\gamma-1} \right) \left(\frac{R_u T_o}{MO_2} \right) \left[1 - \left(\frac{p_e}{p_o} \right)^{\frac{\gamma-1}{\gamma}} \right] \right\}^{1/2} \tag{3.11}$$

where γ is adiabatic gas constant, MO_2 is molecular weight of oxygen, R_u is universal gas constant, T_o is stagnant temperature of gas, and p_e and p_o are the exit pressure and supply pressure of gas, respectively. The pressure at nozzle exit can be determined from

$$\frac{A_t}{A_e} = \left(\frac{\gamma+1}{2} \right)^{\frac{1}{\gamma-1}} \left[\left(\frac{\gamma+1}{\gamma-1} \right) \left\{ \left(\frac{p_e}{p_o} \right)^{\frac{2}{\gamma}} - \left(\frac{p_e}{p_o} \right)^{\frac{\gamma+1}{\gamma}} \right\} \right]^{1/2} \tag{3.12}$$

where A_t and A_e are area of nozzle at throat and at exit, respectively. Eqns (3.10), (3.11) and (3.12) can be used to compute Weber number, We, from Eq. (3.9). The specific iron conversion (defined as Mg/F_{O_2} where F_{O_2} is oxygen flow rate) depends upon Weber number. Deo and Boom [38] have proposed a nomogram between We and Mg/F_{O_2} (Fig. 3.1) which can be used to estimate iron conversion; the variation of iron conversion with lance height for the three typical lance head designs (as given in Table 3.1) is shown Fig. (3.2). The volume fraction of metal in slag can be calculated from

$$\phi_m = \frac{Vl_m}{Vl_m + Vl_s} \tag{3.13}$$

or

$$\phi_m = \frac{Mg(t_r/\rho_m)}{Mg(t_r/\rho_m) + (Ws/\rho_s)} \tag{3.14}$$

where Vl_m and Vl_s are the volume of metal droplets and slag, respectively, and Ws is slag weight; the residence time of metal

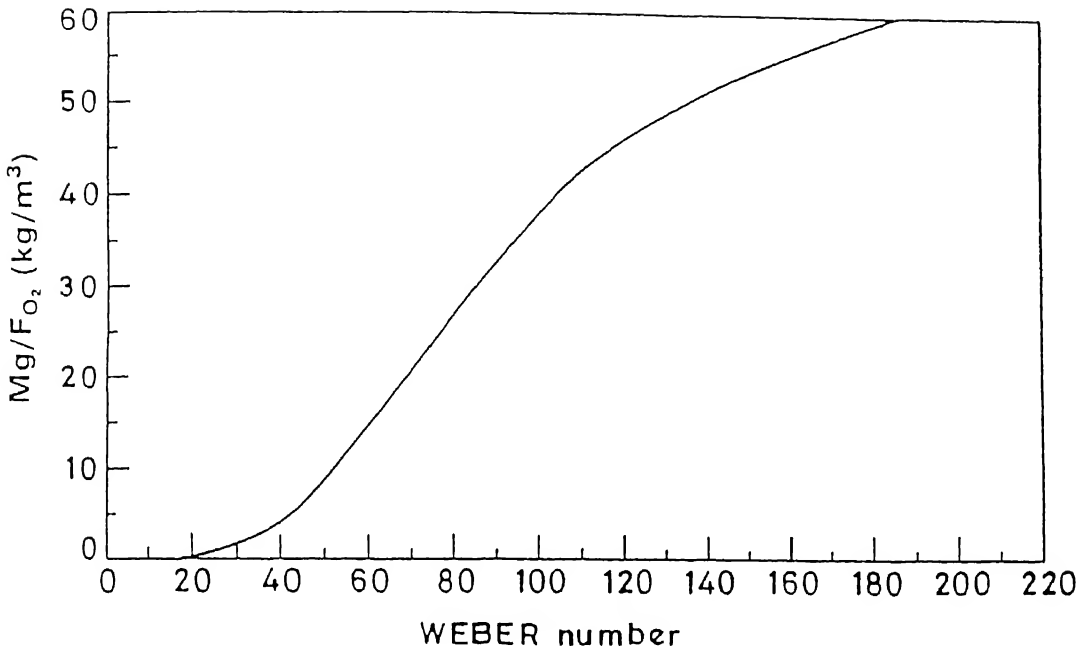

Fig. 3.1 Specific iron conversion versus Weber number [38].

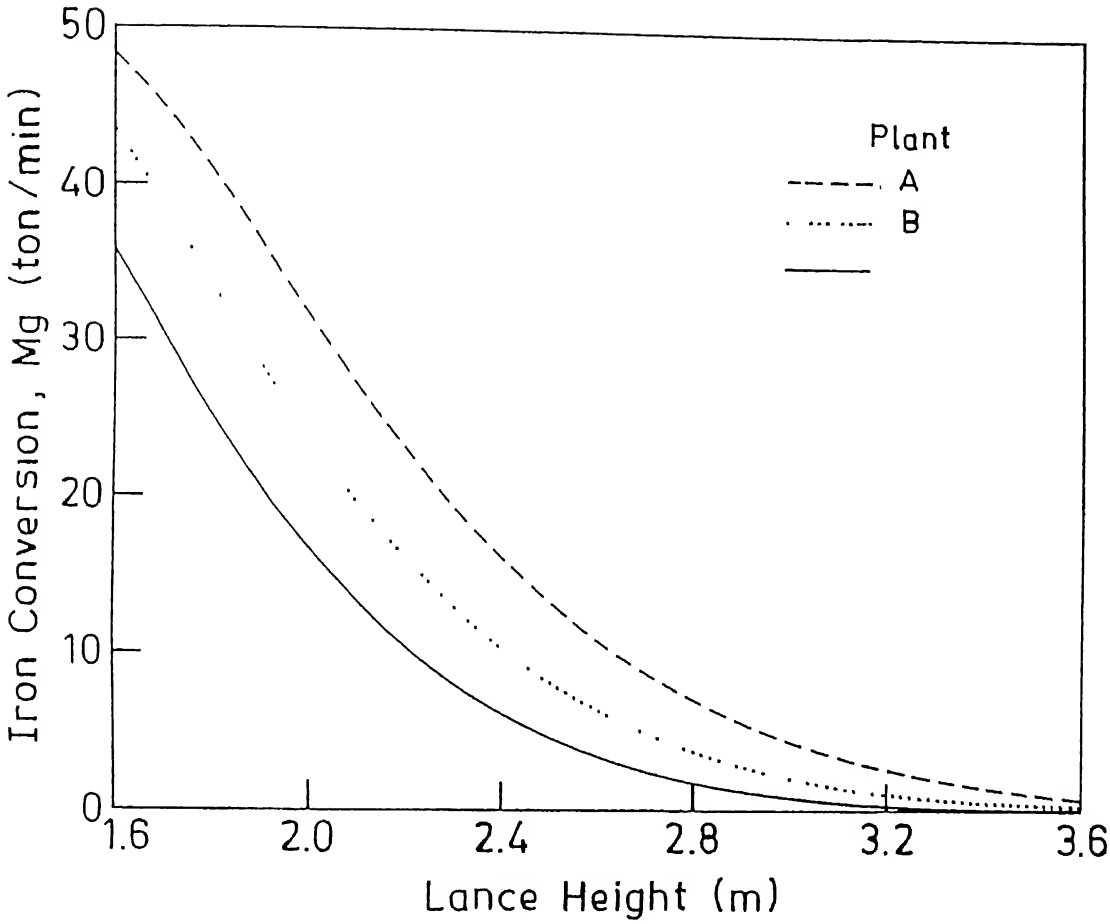

Fig. 3.2 Variation of iron conversion (Mg) with lance height for three different plants (nozzle designs are same as given in Table 3.1)

droplet, t_r, is given by

$$t_r = \frac{h}{V_d} \tag{3.15}$$

It is clear from Eqns (3.4), (3.14) and (3.15) that both ϕ_m and V_d are interdependent and can be evaluated by a simple iterative procedure.

Table 3.1 Lance head design data of three steel plants [38]

Parameters (units)		Plant A	Plant B	Plant C
F_{O_2}	(m^3/min)	900	915	900
p_o	(atm)	11.6	10.8	11.0
d_t	(mm)	48.44	45.2	40.6
d_e	(mm)	63.0	61.3	57.75
θ	(deg)	12	14	14
n		4	5	6
W_{bath}	(tons)	330	315	300

In order to determine the properties of gas-slag continuum (ρ_{sg}, μ_{sg}) and of slag-metal continuum (ρ_{sm}, μ_{sm}) the following procedure is adopted. The ρ_{sg} and ρ_{sm} can be calculated from simple equations

$$\rho_{sg} = \rho_g \phi_g + \rho_s(1-\phi_g) \simeq \rho_s(1-\phi_g) \tag{3.16}$$

where the approximation $\rho_g << \rho_s$ has been made. Further

$$\rho_{sm} = \rho_m \phi_m + \rho_s(1-\phi_m) \tag{3.17}$$

The viscosity of slag-gas (μ_{sg}) and slag-metal (μ_{sm}) continuum can be obtained from Eq.(3.3). In the gas-slag continuum slag is the continuum phase and gas bubbles constitute the dispersed phase. The rising velocity of a gas bubble U_b through the slag is given by

$$U_b = \frac{1}{18} \frac{\left(\rho_s - \rho_g\right) g d_b^2}{\mu_s} \Delta_b \qquad (3.18)$$

where $\Delta_b = \dfrac{3\mu_s \left(1-\phi_g^{1/3}\right)\left(1-\phi_g^{5/3}\right) + \left[3-\frac{9}{2}\left(\phi_g^{1/3}-\phi_g^{5/3}\right)-3\phi_g^2\right]\left(\mu_g+r\right)}{2\mu_s \left(1-\phi_g^{5/3}\right) + \left(3+2\phi_g^{5/3}\right)\left(\mu_g+r\right)}$

U_b also can be expressed in terms of continuum property

$$U_b = \frac{1}{18} \frac{(\rho_{sg} - \rho_s) . g . d_b^2}{\mu_{sg}} \qquad (3.19)$$

By comparing Eqns (3.18) and (3.19) (with an assumption that $\mu_g << \mu_s$ and $r \propto 0$) μ_{sg} is given by

$$\mu_{sg} = \frac{2}{3} \frac{\mu_s}{\left(1-\phi_g^{1/3}\right)} \qquad (3.20)$$

Similarly, the viscosity slag-metal continuum can be estimated from

$$\mu_{sm} = \frac{2\ \mu_s\left(1-\phi_m^{5/3}\right) + \left(3+2\ \phi_m^{5/3}\right)\mu_m}{3\ \mu_s\left(1-\phi_m^{1/3}\right)\left(1-\phi_m^{5/3}\right) + \left[3-\frac{9}{2}\left(\phi_m^{1/3}-\phi_m^{5/3}\right)-3\phi_m^2\right]\mu_m} \qquad (3.21)$$

Using Eqns (3.4), (3.14),(3.16) and (3.20) the droplet velocity, V_d, can be expressed in the form

$$V_d = K_1\ d_m^2 \qquad (3.22)$$

where $K_1 = \frac{1}{18} \frac{(\rho_m - \rho_{sg})}{\mu_{sg}} g\ \Delta_{sm}$

On replacing metal droplet diameter d_m in terms of average droplet diameter d_{avg} (obtained from Eq.(3.6)), Eq.(3.22) can be rewritten as

$$V_d = C \left[\frac{d_t}{x}\right]^{4.824} \qquad (3.23)$$

where $C = K_1\left[0.2x5.513x10^{-6}\left\{10^6\ p_a\left[1.27\left(\frac{p_o}{p_a}\right) - 1\right]\cos\theta\right\}^{1.206}\right]^{2\,0}$

Since it is assumed that all the gas bubbles are of average size, $d_{bcr}/2$, the bubble rise velocity V_g can be determined from Eqns (3.5), (3.7), (3.17) and (3.21)

$$V_g = K_2 \, d_{bcr}^2 \tag{3.24}$$

where $K_2 = \frac{1}{48} \frac{[\rho_{sm} - \rho_g]}{\mu_{sm}} g \left(1-\phi_g^{1/3}\right)$

Now, from Eqns (3.2), (3.23) and (3.24) the final expression for Emulsion number can be written as

$$En = \frac{V_g}{V_d} = \frac{K_2 \, d_{bcr}^2}{C \left[\frac{d_t}{x}\right]^{4.824}} \tag{3.25}$$

or $$En = C' \left[\frac{x}{d_t}\right]^{4.824} \tag{3.26}$$

where $C' = \frac{K_2 \, d_{bcr}^2}{C}$

According to Eqns (3.24) and (3.26), for the given properties of slag-metal-gas emulsion the emulsion number primarily depends upon lance height (x) nozzle throat diameter (d_t) and void fraction (ϕ_g). It is shown in Appendix D that Eq. (3.26) can also obtained from dimensional analysis while using foaming index, Σ, defined by Ito and Fruehan [29]

Let us consider a typical BOF slag (FeO = 15%, CaO = 45%, SiO_2 = 20%, MnO = 8.0%, MgO = 4.0%, Al_2O_3 = 3.0%, CaF_2 = 1.4%, P_2O_5 = 3.6%) and nozzle design of plant-B (given in Table 3.1). The various slag properties, density, surface tension and viscosity, are estimated from different model, as given in Appendix E. The estimated values are:

density of slag	2991.4 kg m^{-3}
surface tension of slag	0.469 kg s^{-2}
viscosity of slag at 1600°C	0.0709 kg $m^{-1}s^{-1}$

The typical values of other parameters, which are needed to estimate emulsion number) are as follows:

σ_m=1.7 kg s^{-2}, ρ_m =7000 kg m^{-3} ρ_g = 0.1821 kg m^{-3} (at 1600°C) μ_m = 0.00568 Pa.s, ξ = 0.44, γ=1.4, Ws = 23000 kg, P_a = 1.0 atm.

Since, the metal fraction, ϕ_m, in emulsion, is found to be very low (of the order of 10^{-3}), the effect coalescence or collision of droplets on their velocity can be neglected, in other words Δ_{sm}= 1.0 in Eq. (3.4).

Figure (3.3) shows the variation of emulsion number with (x/d_t) (values calculated according to Eq. (3.26)) at different gas fractions, ϕ_g. With increase in lance height the maximum droplet size, (d_{llm}) decreases, droplet velocity (V_d) decreases (as evident from Eq.(21)), and hence the emulsion number increases with (x/d_t). It is also evident from Fig. (3.3) that at lower lance heights (< 2m) the effect of ϕ_g is negligible where as at higher lance heights (> 3m) the emulsion number decreases with increasing ϕ_g. It implies that for a given lance head design and supply pressure of oxygen, the constant C′ mainly depends on gas fraction, ϕ_g. For the nozzle of plant B (in Table 3.1) the constant C′ varies with ϕ_g according to the straight line relationship

$$C' = a_1 - b_1.\phi_g \qquad (3.27)$$

where the average value of 'a_1' is 4.14×10^{-10} and that of 'b_1' is 2.012×10^{-10}. In practice, similar equations can be obtained for plants A and C as well.

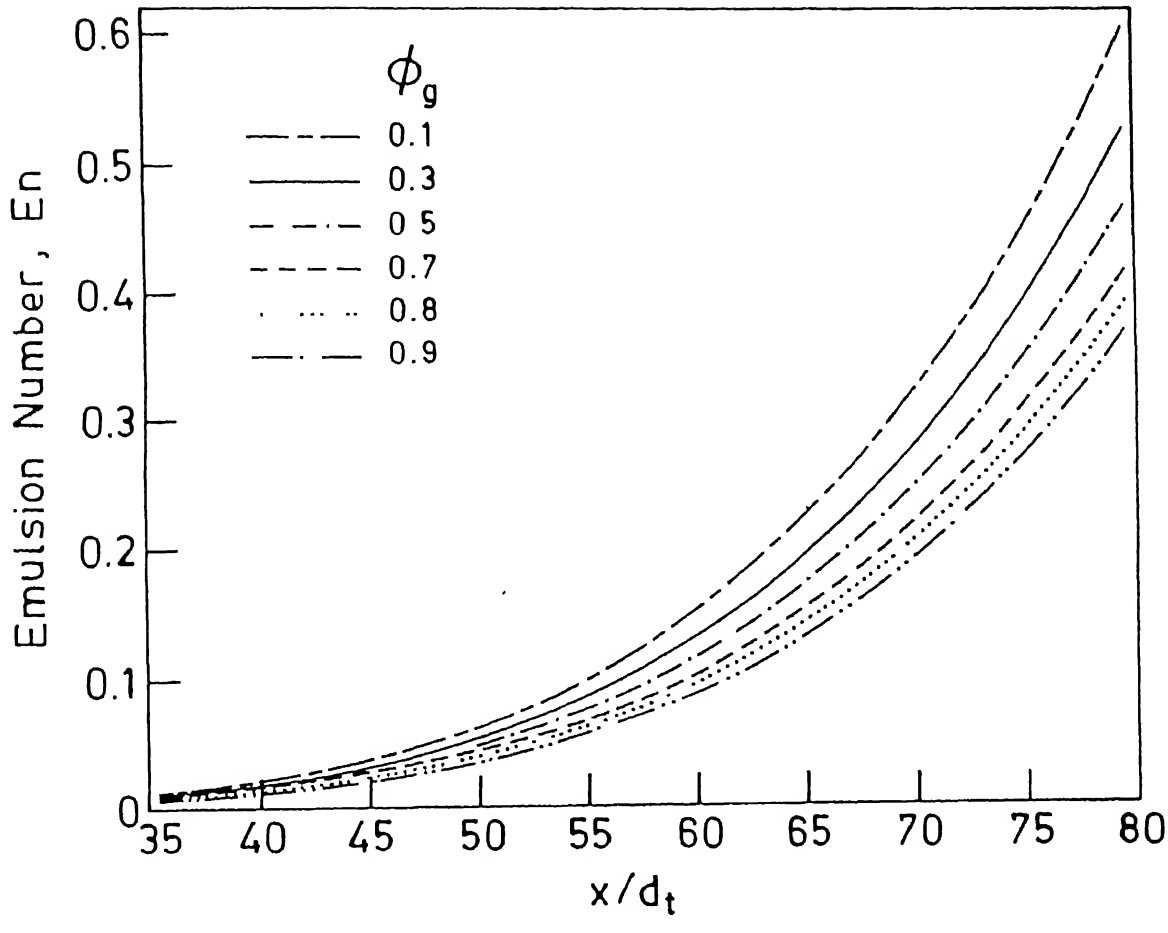

Fig. 3.3 Emulsion number at different ratios of (x/d_t) (lance height to nozzle throat diameter); gas fractions (ϕ_g) varied between 0.1 to 0.9; nozzle design same as that for Plant B in Table 3.1.

3.2 Application of Emulsion number to oxygen steelmaking converters

As an example of application Emulsion number to oxygen steelmaking converters, let us consider the three typical lance nozzle designs in Table 3.1 and the corresponding blowing regimes (the lance height variation pattern with blowing time, Fig. (3.4a)) in oxygen steelmaking converters which were followed at three different steel plants in the recent past [38]. It is interesting to observe from Fig. (3.4b) that the patterns of variation of Emulsion number with process time at all the three plants are very similar to each other implying that emulsion number should be varied only in a small range for a good slag formation.

Emulsion numbers obtained at different lance heights with three different nozzle designs (see Table 3.1 for nozzle design data) are shown in Fig. (3.5). At lance heights less than 2m, the emulsion numbers for plant A, B and C are nearly same (0.04) where as at higher lance heights (greater than 3m) the differences between the three plants A, B and C increase. It implies that at higher lance heights En is very sensitive to operating parameters (including nozzle design).

The supply pressure of oxygen (stagnant pressure of gas before entering the nozzle) affects the metal droplet diameters (Eq. (3.6)) as well as the pressure of oxygen gas at nozzle exit (p_e). In converter operation it is important to maintain supply pressure of oxygen with in a narrow range. However, when two or more converters are simultaneously operating the stagnant pressure may rise or fall. The variation of En with supply pressure of oxygen is shown in Fig. (3.6); at higher lance heights (say >3m) the effect of pressure change

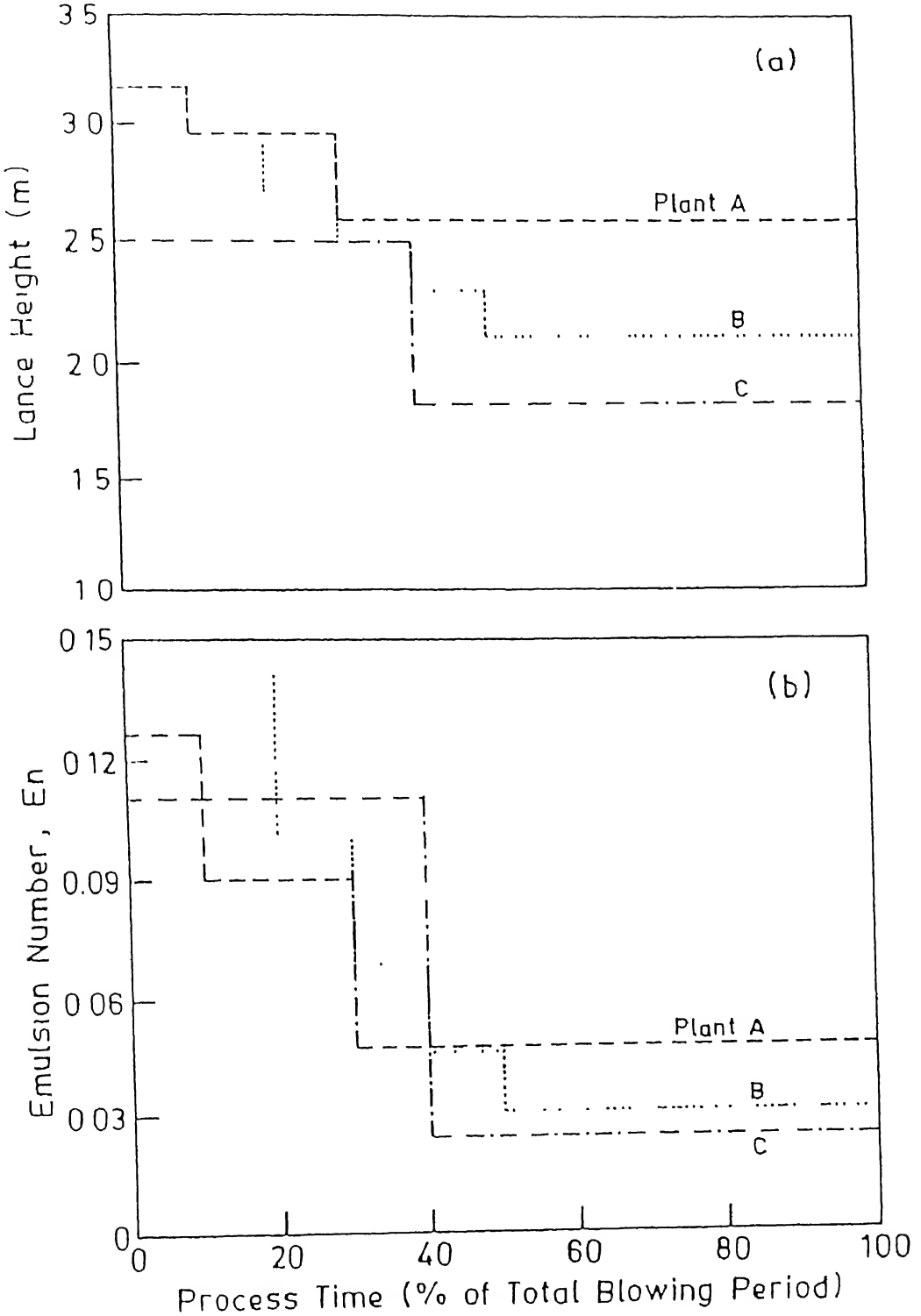

Fig. 3.4 a) Blowing regime (lance height at different times during a blow) practiced at Plants A, B, and C of (Table 3.1)

b) Emulsion number versus process time for Plants A, B, and C (Table 3.1); for $\phi_g = 0.7$.

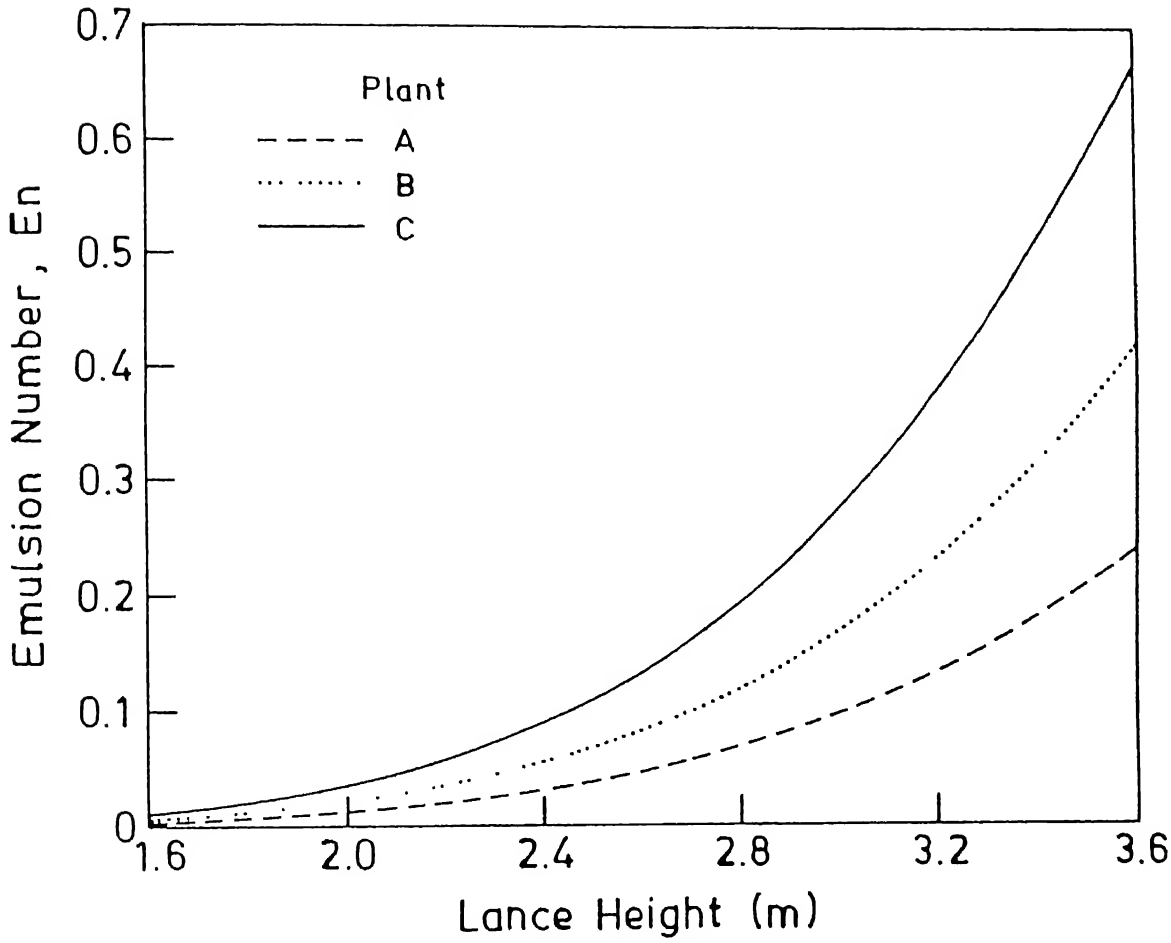

Fig. 3.5 Variation of Emulsion number with lance height for three different nozzle designs (Plants A, B, and C in Table 1); for $\phi_g = 0.7$.

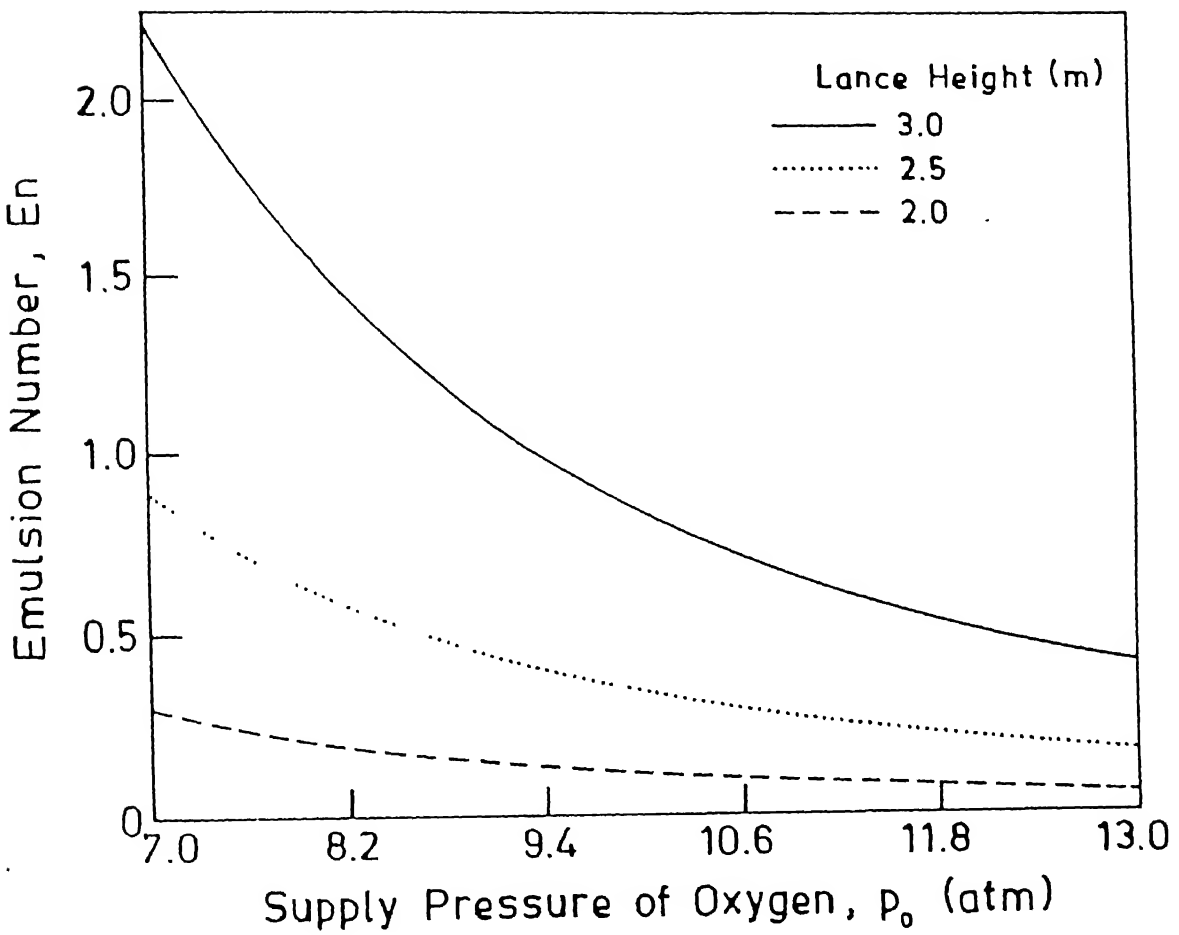

Fig. 3.6 Variation of Emulsion number with supply pressure of oxygen for three different lance heights with ϕ_g = 0.7; nozzle design is same as that of Plant B in Table 3.1.

on emulsion number is relatively more than that at lower lance heights (say 2m).

The rate of reduction of FeO in slag by the metal droplets falling through the slag-gas-metal emulsion formed in oxygen steelmaking converters depends upon the number of metal droplets in slag, residence time of droplets in emulsion, the activity of FeO in slag, mass transfer of FeO in slag, and the chemical reactions taking place at gas-metal and gas-slag interfaces. Under the turbulent conditions (created by the impinging gas jet) the mass transfer of FeO in slag phase can be neglected as a rate controlling step. The overall rate of reduction of FeO in emulsion can then be written from Eq. (2.21) (Sec. 2.1) as

$$-\frac{dn_{FeO}}{dt} = \frac{A.n_{FeO}^{b}}{Vl_s}\left[\frac{1.0}{\frac{1.0}{\alpha.k_2} + \frac{1.0}{\alpha.k_{3a}.K}}\right] \qquad (3.28)$$

where $\alpha = \dfrac{p_{CO}\ \gamma_{FeO}\ Vl_s}{n_{tot}}$

If all the metal droplets are assumed fall through a foam height h, then the residence time of droplets ,t_r is given by Eq. (3.15), as

$$t_r = \frac{h}{V_d}$$

The interfacial reaction area can be calculated from

$$A = \frac{Mg}{\rho_m} \cdot \frac{\text{total area of metal droplets}}{\text{total volume of metal droplets}} \cdot t_r$$

or, $$A = \frac{6\ Mg\ t_r}{\rho_m\ d_{avg}} \qquad (3.29)$$

For the typical BOF slag composition (as mentioned earlier) and the nozzle design of plant-B (given in Table 3.1), the rate of reduction of FeO at 1600°C (calculated with help of Eqns (3.15),

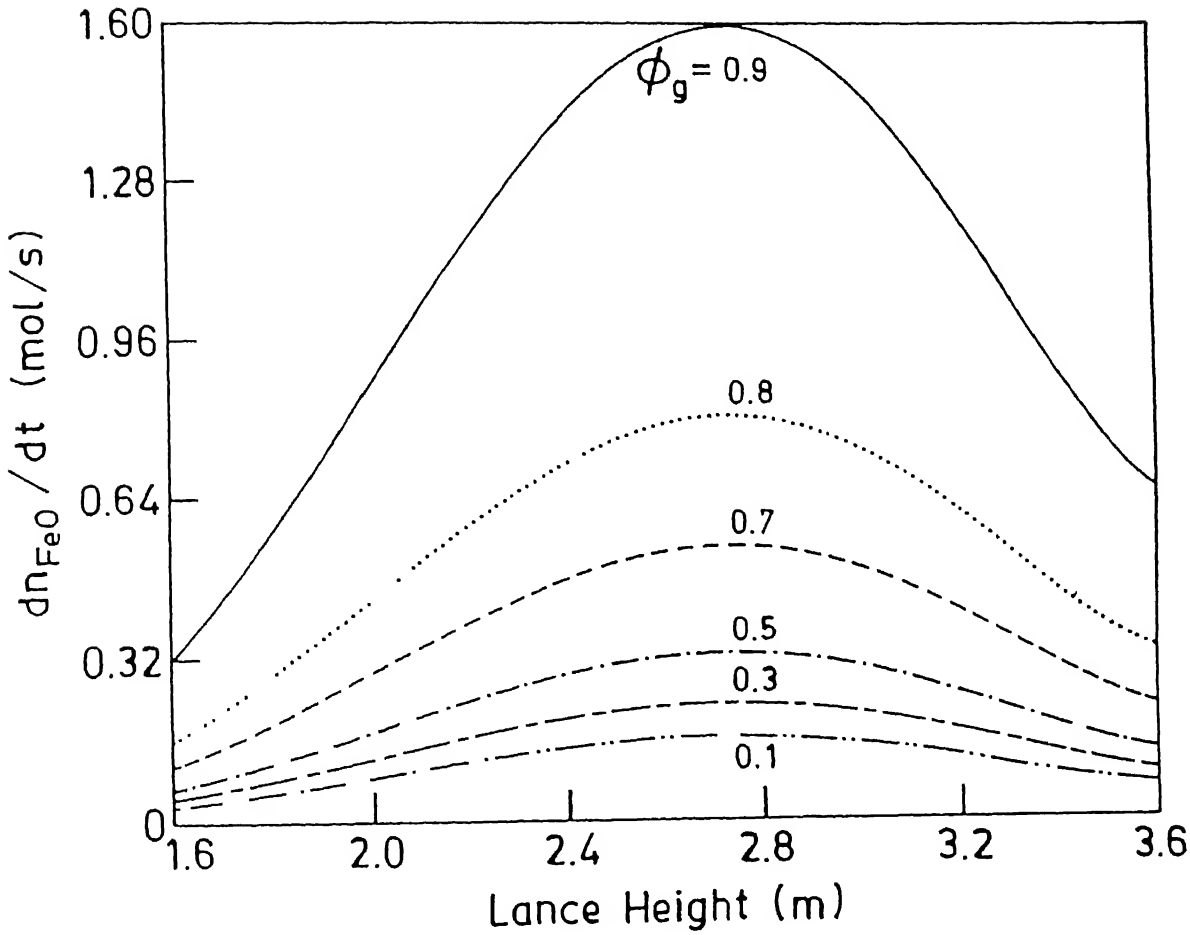

Fig. 3.7 Plot of reduction rate of FeO by metal droplets versus lance height at different gas fractions ϕ_g.

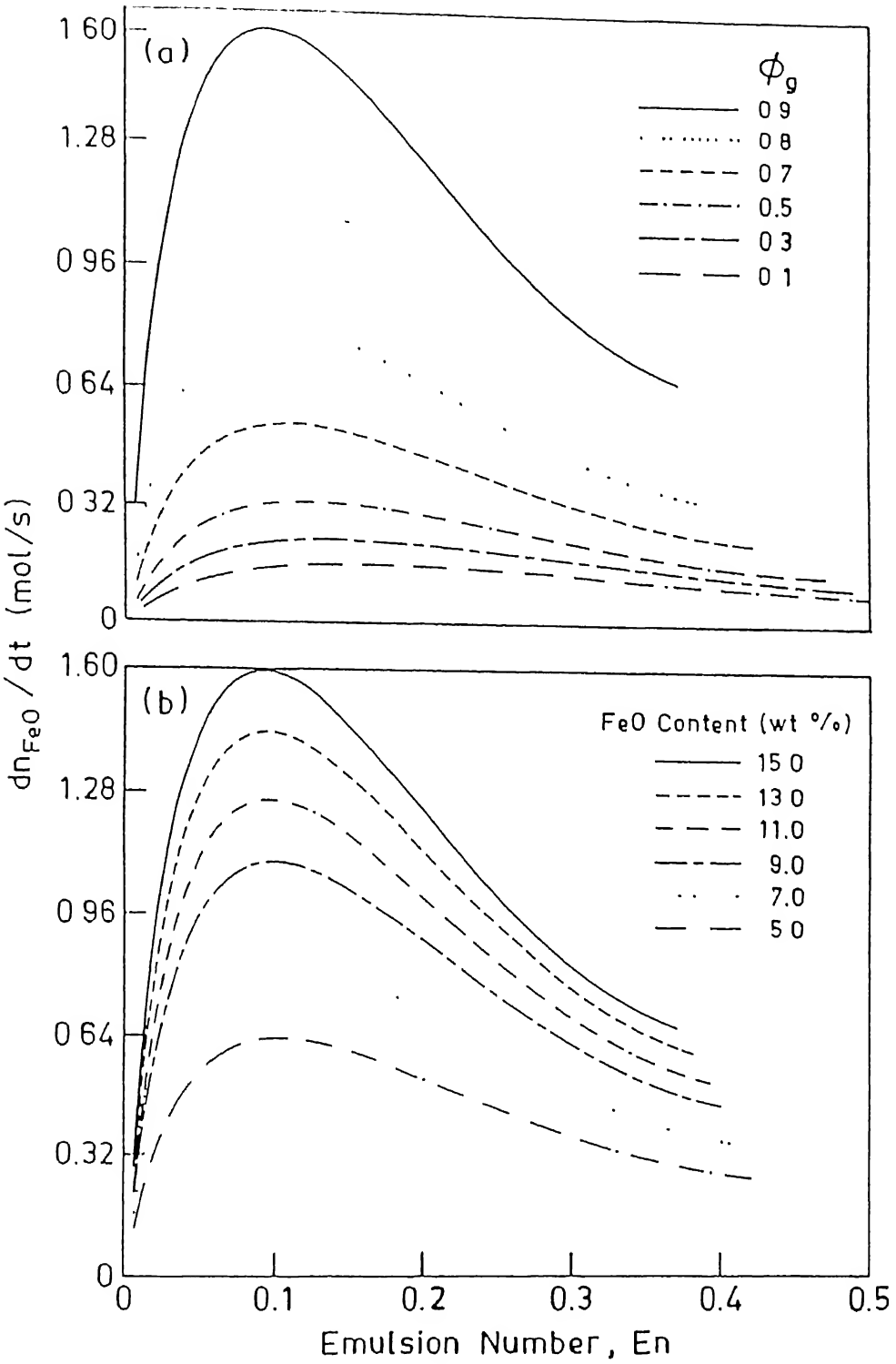

Fig. 3.8 a) Variation of reduction rate of FeO with Emulsion number at different gas fractions (ϕ_g).

b) The effect of FeO content of slag on the reduction rate of FeO at gas fraction $\phi_g = 0.9$

(3.28) and (3.29)) is plotted as a function lance height (Fig. 3.7) and emulsion number (Fig. 3.8a); the effect of FeO content of slag on (dn_{FeO}/dt) is shown in Fig. (3.8b). The reduction rate is maximum when the lance height is in the range of 2.7 to 2.9m (at all gas fractions). Similarly, according to Fig. (3.7a), (dn_{FeO}/dt) is maximum when emulsion number is approximately 0.1. This result can used to control the slag formation behavior, including lime dissolution. For example, a very high rate of reduction of FeO will lead to dry slags because of poor dissolution of lime where as a very low rate of reduction of FeO will increase the attack of FeO on the refractory lining and also increase chances of slopping. From Fig. (3.8b) it can be inferred that control of slag formation is more critical at higher FeO contents when En = 0.1 due to high value of (dn_{FeO}/dt).

CHAPTER 4

CONCLUSIONS

The reduction process of FeO in slags by dissolved carbon in iron-carbon melt (greater than 3 wt% dissolved carbon) has been critically analyzed to understand the governing mechanisms (Chapter 2). The following conclusions can be drown from this study.

1. (i) At low FeO content of the slag (less than 5 wt% FeO) the process is mixed controlled by two steps, namely, mass transfer of FeO in slag and chemical reaction at gas-metal interface (Model-I).

   (ii) At intermediate FeO contents (~ 5 wt% to 40 wt% FeO in slags) the process is controlled by three steps, namely, chemical reaction at gas-metal interface, chemical reaction at gas-slag interface and mass transfer of FeO in slag phase (Model-II).

   (iii) At higher FeO contents (more than 50 wt% FeO) the process tends to become mixed chemical reaction controlled involving chemical reaction at gas-metal interface and chemical reaction at gas-slag interface (Model-III).

2. With the increase of turbulence in slag phase (viz. due to stirring) the process can become mixed chemical reaction controlled (i.e, chemical reaction at gas-metal and gas-slag interfaces) even at lower FeO contents (i.e, less than 40 wt% FeO in slag)
3. The gas-slag chemical reaction rate constant estimated in the present work is given by

$$\ln k_2 = -\frac{32{,}345.4(\pm 6{,}128)}{T} + 19.0(\pm 3.42); \quad \sigma_{\ln k_2, 1/T} = \pm 0.3$$

where k_2 is expressed in mol $m^{-2}s^{-1}bar^{-1}$ and activation energy is 268.9 kJ/mol.

4. Depending upon the FeO concentration in slag and also the experimental conditions the mass transfer coefficient of iron oxide in slag phase is found to vary from 1.0×10^{-5} to 5.0×10^{-5} m/s in the temperature range 1400-1550°C.

The quantitative study of slag-gas-metal droplets emulsion (Chapter 3) has shown that

1. A new dimensionless Emulsion number, En can be expressed in terms of lance height (x) and nozzle throat diameter (d_t)

$$En = C' \left[\frac{x}{d_t} \right]^{4.824}$$

where C′ depends upon system parameters including physical properties of slag and gas void fraction in slag.

2. It is observed that successful blowing regimes followed in oxygen steelmaking converters at different steel plants are such that the pattern of variation of Emulsion number with process time are nearly same. The emulsion number should be controlled with in critical limits (0.05-0.1) (Fig. 3.8) for a good slag formation, minimize refractory lining wear and also decrease chances of slopping.

3. The effect of employing new blowing regimes or new lance nozzle designs on slag formation can be quantified in terms of Emulsion number. This will also help to reduce the number of trial and error runs needed to arrive at the optimum blowing regime for a given grade of steel.

REFERENCES

1. *Mulholland, E.W.; Hazledean, G.S.F.; Davies, M.W.:* Jl. Iron Steel Inst., Vol. 211 (1973), p. 632/39

2. *Ooi, O.; Nozaki, T.; Yoshi, H.:* Transactions ISIJ, Vol. 14 (1974), p. 9/16

3. *Sommerville, I.D.; Grieveson, P.; Taylor, J.:* Ironmaking and Steelmaking, Vol. 7 (1980), p. 25/32

4. *Hasham, Ali; Pal, U.B.; Krishna Murty, G.G.:* EPD Congress '92, Edited by J.P.Hager, 1992, Warrendale, PA, Metallurgical Socity of AIME, p. 847/65.

5. *Sawada, Y; Krishna Murthy, G G; Elliott, J.F.:* EPD Congress '92 Edited by J.P. Hager. The Minerals Metal & Materials Society. 1991. p. 915/25

6. *Hacioglu, M.; Pomfret, R. J.:* Department of Metallurgy, University of Strathclyde, Glasgow Scotland, Personnel communication.

7. *Sato, A.; Aragane, G.; Kamihira, K.; Yoshimatsu, S.:* Transactions ISIJ, Vol. 27 (1987), p. 789/96

8. *Sato, A.; Aragane, G.; Hirose, F.; Nakagawa, R.; Yoshimatsu, S.:* Transactions ISIJ, Vol. 24 (1984), p. 808/15.

9. *Wei, P.; Sano, M.; Hirasawa, M.; Mori, K.:* ISIJ International, Vol. 31 (1991), p. 358/65

10. *Wei, P.; Sano, M.; Hirasawa, M.; Mori, K.:* Transactions ISIJ, Vol. 28 (1988), p. 637/44

11. *Bafghi, S.M.; Ito, Y; Yamada, S; Sano, M.:* ISIJ International, Vol. 32 (1992), p. 1084/90

12. *Bafghi, S.M.; Ito, Y.; Yamada, S.; Sano, M.:* ISIJ International, Vol. 32 (1992), p. 1280/86.

13. *Sugata, M; Sugiyama, T; Kondo, S.:* Transactions ISIJ, Vol. 14 (1974), p. 88/95

14. *Nagasaka, T.; Iguchi, Y.; Ban-ya, S.:* Fifth International Iron and Steel Congress, The Iron and Steel Society (AIME) April 6-9, 1986, Volume 6, Book 3 (1986), p. 669/78

15. *Fine, H.A.; Meyer, D.; Janke, D.; Engell, H.J.:* Ironmaking and Steelmaking, Vol. 12 (1985), p. 157/62

16. *Dancy, T.E.:* Jl. Iron and Steel Inst., Sept. 1951, p. 17/23

17. *Sain, D.R.; Belton, G.R.:* Metallurgical Transactions B, Vol. 7B (1976), p. 235/44

18. *Mannion, F.J.; Fruehan, R.J.:* Metallurgical Transactions B, Vol. 20B (1989), p. 853/61

19. *Turner, G.; Jahanshahi, S.* : Transactions ISIJ, Vol. 27 (1987), p.734/39

20. *Katayama, H.; Ibaraki, T.; Ohno, T.; Yamauchi, M.; Hirata, H.; Inomoto, T.* : ISIJ International, Vol.33 (1993), p. 124/32

21. *Wei, T.; Oeters, F.* : Int. Symposium on Injection in Process Metallurgy, The Minerals, Metals & Materials Society, 1991, p. 143/64

22. *Standish, N.; He, Q.L.* : ISIJ International, Vol. 29 (1989), p. 455/61

23. *He, Q.L.; Standish, N.* : ISIJ International, Vol. 30 (1990), p. 305/9

24. *He, Q.L.; Standish, N.:* ISIJ International, Vol. 30 (1990), p. 356/6125. *Gal-Or, B.; Waslo, S.* : Chem. Engg. Science, 1968, Vol. 23, p. 1431/46

26. *Hatzikiriakos, S.G.; Gaikwad, R.P.; Nelson, P.R.; Shaw, J.M.* : AIChE Journal., Vol. 36 (1990), p. 677/84

27. *Ogawa, Y.; Katayama, H.; Hirata, H.; Tokumitsu, N.; Yamauchi, M.* : ISIJ International, Vol. 32 (1992), p. 87/94

28. *Ito, K.; Fruehan R.J.* : Metalllurgical Transactions B, Vol. 20B (1989), p. 509/14

29. *Ito, K.; Fruehan R.J.* : Metalllurgical Transactions B, Vol. 20B (1989), p. 514/21

30. *Roth, R.E.; Jiang, R.; Fruehan, R.J.* : Iron & Steelmaker, Transactions of the ISS, November 1992, p.55/63

31. *Koria, S.C.; Lange, K.W.:* Ironmaking and Steelmaking, Vol. 13

(1986), p. 236/40

32. *Ogawa, Y.; Huin, D.; Gaye, H.; Tokumitsu, N.*: ISIJ Int., Vol. 33 (1993), p. 224/32

33. *Cramb, A.W.; Belton, G.R.:* Metallurgical Transactions B, 12B (1981) p. 699/704

34. *Ban-ya, S.:* ISIJ International, Vol. 33 (1993), p. 2/11

35. *Gaskell, D.R.:* Introduction to Metallurgical Thermodynamics, Scripta Book Company, Washington D.C. (U.S.A), 1973

36. *Tarby S.K.; Philbrook, W.O.:* Transactions AIME, Vol. 239 (1967), p. 1005/17

37. *Borgianni, C.:* Ironmaking and Steelmaking, Vol. 5 (1978), p. 61/66

38. *Deo, B.; Boom, R.:* Fundamentals of Steelmaking Metallurgy, Prentice Hall, U.K., 1993.

39. *Mills, K.C.; Keene, B.J.:* International Materials Reviews, Vol. 32 (1987), p. 105/8

40. *Urbain, G.* : Steel Research, Vol. 58 (1987), p. 111/16

APPENDIX - A

DETERMINATION OF ACTIVITY COEFFICIENT OF FeO IN SLAGS

According to the regular solution model the activity coefficient of component, i, in a multi-component regular solution is expressed by following equations [34]

$$\bar{G}_i^E = \Delta\bar{H}_i = RT \ln \gamma_i \tag{A1}$$

$$RT \ln \gamma_i = \sum a_{ij} X_j^2 + \sum \sum (a_{ij} + a_{ik} - a_{jk}) X_j X_k \tag{A2}$$

where $\bar{G}_i^E$ is the excess partial molar free energy, $\Delta\bar{H}_i$ is the relative partial molar enthalpy, X_j and X_k are the respective fractions of the cation species j and k and a_{ij} is the interaction energy between cations i.e, (i cation)-O-(j cation). The values of interaction energy parameters (a_{ij}) for CaO-FeO-Al_2O_3-SiO_2 slags are given in Table A1. From Eq. (A2) the value of γ_{FeO} for CaO-FeO-Al_2O_3-SiO_2 slags can be calculated from

$$RT \ln \gamma_{FeO} = -41840 X_{SiO_2}^2 - 31380 X_{CaO}^2 - 41000 X_{Al_2O_3}^2 + 60670 X_{SiO_2} X_{CaO} + 44770 X_{SiO_2} X_{Al_2O_3} + 82430 X_{CaO} X_{Al_2O_3} \tag{A3}$$

In the above equation the reference state of stoichiomatric FeO is taken as regular solution; the standard state is pure liquid iron oxide in equilibrium with metallic iron. The standard free energy involved in the change of reference state is given by [34]

$$Fe_tO + (1-t)\ Fe(s \text{ or } l) = FeO\ (R.S) \tag{A4}$$

$$_d\Delta G^\circ = -8540.0 + 7.142\ T\ (J) \tag{A5}$$

So by knowing the regular solution activity, a_{FeO}(R.S.), the Raoultian

activity can be calculated from

$$RT \ln a_{Fe_tO\ (l)} = RT \ln a_{FeO\ (R.S)} - 8540.0 + 7.142\ T\ (J) \qquad (A6)$$

Thus from Eqns (A3) and (A6) expression for $\gamma_{Fe_tO(l)}$ can be obtained as

$$RT\ln \gamma_{Fe_tO(l)} = -41840\ X^2_{SiO_2} - 31380\ X^2_{CaO} - 41000\ X^2_{Al_2O_3} + 60670\ X_{SiO_2} X_{CaO} + 44770\ X_{SiO_2} X_{Al_2O_3} + 82430\ X_{CaO}\ X_{Al_2O_3} - 8540.0 + 7.142\ T\ (J) \qquad (A7)$$

According to Eq.(A7), at 1793K and for slag containing X_{SiO_2}=0.436, X_{CaO}= 0.459 $X_{Al_2O_3}$ = 0.0615 and X_{FeO}= 0.0422 (this slag was employed by Sato *et al.* [8]), the value of $\gamma_{Fe_tO(l)}$ is 1.4188.

The activity coefficient of FeO in CaO-FeO-Li_2O-SiO_2 slags (i.e, slag containing Li_2O) was taken from the work of Wei *et al.* [10] (γ_{FeO}= 3.2). This is because the interaction energy data between $Fe^{2+}$and Li^+ and $Ca^{2+}$and Li^+ cations are not available.

Table A1 Interaction energy between cations of major components in steelmaking slag, a_{ij} (J) [34].

i \ j	Fe^{2+}	Fe^{3+}	Mn^{2+}	Ca^{2+}	Mg^{2+}	Si^{2+}	P^{5+}	Al^{3+}
Fe^{2+}	——	-18660	+7110	-31380	+33470	-41840	-31380	-41000
Fe^{3+}	-18660	——	-56480	-95810	-2930	+32640	+14640	-161080
Mn^{2+}	+7110	-56480	——	-92050	+61920	-75310	-84940	-83680
Ca^{2+}	-31380	-95810	-92050	——	-100420	-133890	-251040	-154810
Mg^{2+}	+33470	-2930	+61920	-100420	——	-66940	-37660	-71130
Si^{2+}	-41840	-32640	-75310	-133890	-66940	——	+83680	-127610
P^{5+}	-31380	+14640	-84940	-251040	-37660	+83860	——	-261500
Al^{3+}	-41000	+161080	-83680	-154810	-71130	-127610	-261500	——

APPENDIX - B

CALCULATION OF RATE CONSTANTS (k_2 AND k_{FeO})

To calculate the mass transfer coefficient of FeO in slag (k_{FeO}), or reaction rate constant k_2, the experimental data of FeO reduction are plotted in terms of $-\ln (FeO_o/FeO_t)$ vs. time, as shown in Fig. (B1). According to equation Eq. (2.19) the slope of the plotted straight line (when all three steps are rate controlling, Model-II), will be equal to

$$\text{slope} = \frac{A}{V}\left[\frac{1.0}{\frac{1}{\alpha.k_2} + \frac{1}{\alpha.K.k_{3a}} + \frac{1}{k_{FeO}}}\right] \qquad \text{(B1)}$$

By substituting various parameters of Eq. (B1), the reaction rate constant k_2 or mass transfer coefficient k_{FeO} can be determined.

For example, from the experimental data of Sommerville *et al.* the slope of the plot of $-\ln\left\{\frac{FeO_t}{FeO_o}\right\}$ against time (Fig. B1) is 0.051. The experimental parameters were

area of slag/metal interface	6.5 cm^2
density of slag	2.6 g cm^{-3}
volume of slag	11.83 cm^3

At 1380°C the equilibrium constant (K) of reaction (1.2) is equal to 0.1228 and reaction rate constant k_{3a} is 5.15 mol $m^{-2}s^{-1}bar^{-1}$. So from Eq. (2.20) in which chemical reaction at gas-metal interface and mass transfer FeO in slag phase are rate controlling, value of k_{FeO} is given by

$$k_{FeO} = \frac{slope.V.\alpha.K.k_{3a}}{(A.\alpha.K.k_{3a} - V.slope)} \qquad (B2)$$

By substituting above values in Eq. (B2) the mass transfer coefficient of FeO in a slag containing 2.5 wt% FeO is $k_{FeO} = 2.20 \times 10^{-5}$ m/s.

The various experimental parameters and coefficients used to calculate rate constant or mass transfer coefficient are summarized in Table B1.

Table B1 Various experimental parameters and coefficients used for calculation of rate constant or mass transfer coefficient.

Ref.	FeO content (wt%)	Reaction area (cm^2)	Volume of slag (cm^3)	Density of slag g cm^{-3}	γ_{FeO}	Slope
Sommer-ville et al.[3]	1.53	6.5	11.5	2.6	1.6624	0.056
	2.50	6.5	11.83	2.6	1.6507	0.051
	3.17	6.5	11.9	2.6	1.6450	0.048
Hasham et al[4]	5.60	2.0978	48.07	2.6	1.4657	0.005
	4.50	3.5872	48.07	2.6	1.4497	0.0085
Sato et al. [8]	5.0	23.75	16.19	2.5	1.4188	0.077
	10.0	23.75	17.09	2.5	1.4105	0.113
	20.0	23.75	19.23	2.5	1.3955	0.104
	30.0	23.75	21.97	2.5	1.3821	0.1036
	40.0	23.75	25.64	2.5	1.3856	0.1205
	50.0	23.75	30.76	2.5	1.3703	0.1238
Wei et al [9]	10.0	18.84	14.28	2.45	3.2	0.1195
	15.0	18.84	14.28	2.45	3.2	0.1259
	20.0	18.84	14.28	2.45	3.2	0.1307

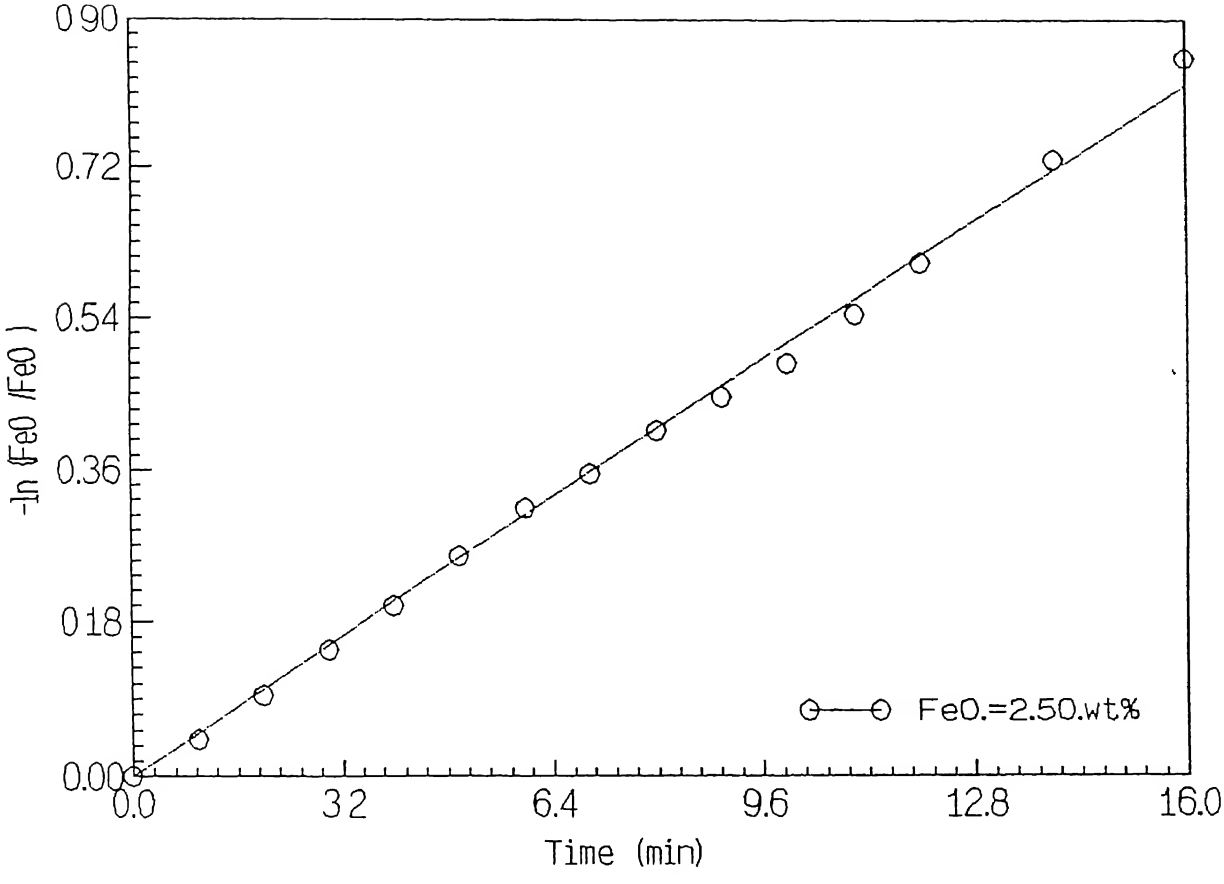

Fig. B1 Plot of $-\ln (FeO_t/FeO_o)$ versus time.

APPENDIX - C

CALCULATION OF AVERAGE DIAMETER OF DROPLETS (d_{avg})

In a top-blown oxygen steelmaking converter the fraction f(d) of droplets of diameter, d, due to an impinging supersonic jet is assumed to follow the Rosin-Rammler-Sperling (RRS) distribution [31]

$$f(d) = 8.7038\ RF\ \frac{d^{0.26}}{d_{lim}^{1.26}} \tag{C1}$$

where RF is the droplet size distribution, in fractions and

$$RF = (0.001)^{\left(\frac{d}{d_{lim}}\right)^{1.26}} \tag{C2}$$

or,
$$RF = e^{-6.908\left(\frac{d}{d_{lim}}\right)^{1.26}} \tag{C3}$$

The maximum size of droplet produced, d_{lim}, is given by [31]

$$d_{lim} = 5.513\ X\ 10^{-6}\left[10^{6}\left(\frac{d_t}{x}\right)^{2} p_a \left[1.27\left(\frac{p_o}{p_a}\right) - 1\right] \cos\theta\right]^{1.206} \tag{C4}$$

Relationship between d_{lim} and $\bar{d}_{avg}$

The value of d_{lim} can be used to calculate the average diameter of the distribution (d_{avg}) as follows

$$d_{avg} = \int_{0}^{d_{lim}} d\ f(d)\ \delta d \tag{C5}$$

Substituting for f(d) from Eqns (C1) and (C3)

$$d_{avg} = 8.7038 \int_0^{d_{llm}} \left(\frac{d}{d_{llm}}\right)^{1.26} e^{-6.908\left(\frac{d}{d_{llm}}\right)^{1.26}} \delta d \qquad (C6)$$

Let $$p = 6.908 \left(\frac{d}{d_{llm}}\right)^{1.26}$$

Thus, we get :

$$d_{avg} = \frac{8.7038\, d_{llm}}{6.908^{(2.26/1.26)} 1.26} \int_0^{6.908} p^{1/1.26} e^{-p}\, dp \qquad (C7)$$

On integrating Eq. (C7) by Simpson's rule

$$d_{avg} = 0.2\, d_{llm} \qquad (C8)$$

The variation of average metal droplets size with lance height for Plant B (Table 3.1) is shown in Fig. C1.

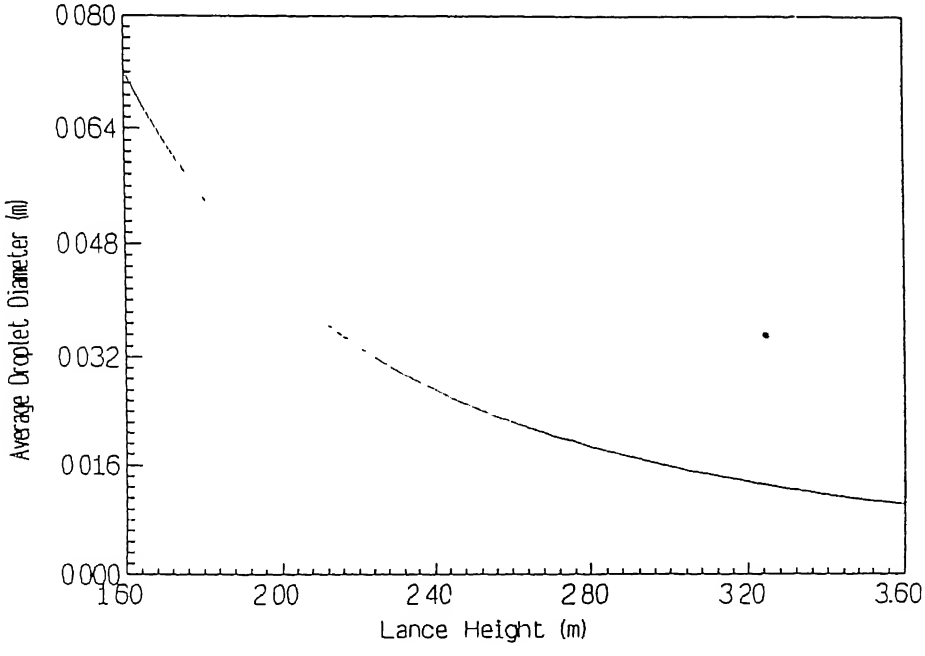

Fig. C1 Effect of change in lance height on average metal droplet size for Plant B (Table 3.1)

APPENDIX - D

DERIVATION OF EMULSION NUMBER FROM DIMENSIONAL ANALYSIS

Velocity of an ensemble of droplets falling through gas-slag dispersion depends upon the physical properties of the system

$$V_d = f(\mu_m, \mu_s, d_m, \rho_m, \rho_s, g, \phi_m, \phi_g) \quad (D1)$$

By employing the Buckingham π theorem, Eq. (D1) can be rearranged in a dimensionless form

$$Re_d = f\ (D_1, D_2, D_3, \phi_m, \phi_g) \quad (D2)$$

where Re_d is the Reynolds number for the droplet and is defined as

$$Re_d = \frac{\rho_s\ d_m V_d}{\mu_s} \quad (D3)$$

and dimensionless numbers D_1, D_2 and D_3 appearing in Eq. (D2) are given by

$$D_1 = \frac{\rho_m}{\rho_s} \quad (D4)$$

$$D_2 = \frac{\mu_m}{\mu_s} \quad (D5)$$

$$D_3 = \frac{g\ \rho_s^2\ d_m^3}{\mu_s^2} \quad (D6)$$

It should be noted that V_d (appearing in Eq. (D3)) represents the settling velocity of a metal droplet through gas-slag dispersion in the presence of other droplets. By introducing dimensionless groups from Eqns (D3)-(D6), slag-gas continuum properties ρ_{sg} and μ_{sg} from Eqns (3.16) and (3.20) respectively, and droplet velocity from Eq. (3.4) the Reynolds number for metal

droplets, Re_d, can be written as

$$Re_d = \frac{1}{12}\left(D_1+\phi_g-1\right) D_3 \left(1-\phi_g^{1/3}\right) \varepsilon \tag{D7}$$

where $$\varepsilon = \frac{\left[\frac{2\left(1-\phi_m^{1/3}\right)}{\left(1-\phi_g^{1/3}\right)}\left(1-\phi_m^{5/3}\right) + \left[3-\frac{9}{2}\left(\phi_m^{1/3}-\phi_m^{5/3}\right)-3\phi_m^2\right] D_2\right]}{\left[\frac{4\left(1-\phi_m^{5/3}\right)}{3\left(1-\phi_g^{1/3}\right)} + D_2\left(3+2\phi_m^{5/3}\right)\right]}$$

In order to delineate the significant variables in Eq. (D7), an extensive parametric study was undertaken to evaluate the dependence of Re_d on each of the dimensionless groups appearing on right hand side of Eq. (D7). Only one variable was changed at a time. In this manner, it was established that Re_d (which incorporates V_d) was primarily determined by the value of D_3; thus

$$Re_d = a\ D_3 \tag{D8}$$

From Eq. (D9) where the value of parameter 'a' is given by

$$a = \frac{1}{12}\left(D_1+\phi_g-1\right)\left(1-\phi_g^{1/3}\right)\varepsilon \tag{D9}$$

Ito and Fruehan [10] have defined Foaming Index, Σ, as

$$\Sigma = \frac{h}{V_g} \tag{D10}$$

Based on experimental observations they further correlated the foaming index with the physical properties of the slag as follows

$$\Sigma = k\frac{\mu_s}{\sqrt{\rho_s \sigma_s}} \tag{D11}$$

Note that Σ is defined for a gas-slag mixture only and k is a dimensional constant. It is possible to express h/V_g in Eq. (D10) in terms of slag properties via Eq. (D11).

On rewriting Eq.(D11) in terms of effective values of density, viscosity and surface tension for the slag-metal droplet-gas emulsion

$$\Sigma = k \frac{\mu_{eff}}{\sqrt{\rho_{eff}\ \sigma_{eff}}} \tag{D12}$$

Equations (3.2), (D3), (D6), (D8), (D10) and (D11) can easily be combined to yield a completely predictive expression for Emulsion number, En, as a function of the pertinent system and physical variables.

From Eqns (D10) and (D12)

$$V_g = \frac{h}{k\ \mu_{eff}} \sqrt{\rho_{eff}\ \sigma_{eff}} \tag{D13}$$

Now, from Eqns (D3), (D6) and (D8)

$$Re_d = \frac{\rho_{eff}\ d_m V_d}{\mu_{eff}} = \frac{a\ g\ \rho_{eff}^2\ d_m^3}{\mu_{eff}^2} \tag{D14}$$

On simplifying

$$V_d = \frac{a\ g\ \rho_{eff}\ d_m^2}{\mu_{eff}} \tag{D15}$$

From Eqns (3.2), (D13) and (D15)

$$En = \frac{h}{a\ k\ g} \sqrt{\frac{\sigma_{eff}}{\rho_{eff}}}\ \frac{1}{d_m^2} \tag{D16}$$

On replacing d_m with d_{avg} and noting that $d_{avg} = 0.2\ d_{lim}$ (see Appendix C), we get

$$En = \frac{25\ h}{a\ k\ g} \sqrt{\frac{\sigma_{eff}}{\rho_{eff}}}\ \frac{1}{d_{lim}^2} \tag{D17}$$

or $$En = C_1 \left[\frac{x}{d_t}\right]^{4\,824} \tag{D18}$$

where $$C_1 = \frac{25\ h}{a\ k\ g\ c^2} \sqrt{\frac{\sigma_{eff}}{\rho_{eff}}}$$

and $$c = 5.513\ X\ 10^{-6}\left[10^6\ p_a\left[1.27\left(\frac{p_o}{p_a}\right) - 1\right]\cos\theta\right]^{1.206}$$

The expression for emulsion number in Eq. (D18) is, in principle, similar to that in Eq. (3.26). However, Eq. (D18) contains the term foam height, h, which can be determined from experimental observations only. In the present work for the sake of convenience Eq. (3.26) has been used for analysis because it does not contain the foam height.

APPENDIX - E

ESTIMATION OF PROPERTIES OF SLAGS (ρ, σ, AND μ)

E1. Model for Estimating the Density (ρ) of Slags

An additive method is used for the estimating the density of slags. For example, the density of slag, with three oxide constituents, is given by

$$\rho_s = \frac{M_1X_1 + M_2X_2 + M_3X_3}{V} \qquad \text{(E1)}$$

where V is the molar volume of slag, X is the mole fraction of oxide constituent, M is the molecular weight of oxides and the subscripts 1, 2 and 3 denote the various oxide constituents of slag. The molar volume of slag can be determined from partial molar volume of oxides, V′, as follows:

$$V = X_1V_1' + X_2V_2' + X_3V_3' \qquad \text{(E2)}$$

The Eq. (E1) and (E2) can also be generalized for more than three constituents of slag. The values of partial molar volume of various slag constituents considering the structure of slag, as recommended by Mills and Keene [39], are given in the Table E1.

For a typical BOF slag (FeO = 15.0%, CaO = 45.0% SiO_2= 20.0%, MnO = 8.0%, MgO = 4.0%, Al_2O_3 = 3.0%, CaF_2 = 1.4%, P_2O_3 = 3.6%, all are in wt%) the estimated value of slag density is 2991.4 kg m^{-3}.

E2. Model for Estimating the Surface Tension (σ) of Slags

Model for estimating the surface tension of slags, as based on the addition of the partial molar contributions σ' of the

individual constituents, have been reported in the review work of Mills and Keene [39]. According to this method surface tension of slag can be estimated as follows:

$$\sigma = X_1\sigma'_1 + X_2\sigma'_2 + X_3\sigma'_3 + \ldots \qquad \text{(E3)}$$

where the subscripts 1,2,3 etc. denote the various slag constituents. The partial surface tension for non-surface-active constituents are given in Table E2 and the equations for calculating σ' for surface-active components, which depends on its mole fraction, are given in Table E3.

For the above BOF slag composition the surface tension is estimated from Eq. (E3) and found to be 0.469 kg s^{-2}

Table E1 Partial molar volume (V') of various slag constituents at 1500°C [39]

Constituents	V', $cm^3 mol^{-1}$
Al_2O_3	$28.31 + 32\ X_{Al_2O_3} - 31.45\ X^2_{Al_2O_3}$
CaF_2	31.3
CaO	20.7
FeO	15.8
Fe_2O_3	38.4
MgO	16.1
MnO	15.6
P_2O_5	65.7
SiO_2	$19.55 + 7.966\ X_{SiO_2}$

E3. Model for Estimating Viscosity (μ) of Slags

The viscosity of slag was estimated from the model given by Urbain [41] which follows the Frankel equation of viscosity:

$$\mu = AT \exp (B/T) \qquad \text{(E5)}$$

where A and B are the viscosity parameters, T is the thermodynamic temperature (K) and μ is in $Nm^{-2}s$.

Table E2 Partial molar surface tension σ' for different non surface-active slag constituents at 1500°C [39]

Oxide	Al_2O_3	CaO	FeO	MgO	MnO	SiO_2	TiO_2
σ', mNm^{-1}	655	625	645	635	645	260	360

In this model the parameters A and B are calculated by dividing the slag constituents into three categories:

(i) 'glass formers', $X_G = X_{SiO_2} + X_{P_2O_5}$

(ii) 'modifiers', $X_M = X_{CaO} + X_{MgO} + X_{Na_2O} + X_{K_2O} + 3X_{CaF_2} + X_{FeO} + X_{MnO} + 2X_{TiO_2} + 2X_{ZrO_2}$

(iii) 'amphoterics', $X_A = X_{Al_2O_3} + X_{Fe_2O_3} + X_{B_2O_3}$

In the present work, Fe_2O_3 has been classified as a modifier and in the computer program $1.5\ X_{FeO_{1.5}}$ has been added to X_M and $X_{Fe_2O_3}$ deducted from X_A. 'Normalized' values X_G^*, X_M^*, and X_A^* are obtained by dividing the mole fractions, X_G, X_M and X_A by the term $(1 + 2X_{CaF_2} + 0.5X_{FeO_{1.5}} + X_{TiO_2} + X_{ZrO_2})$. Urbain [40] proposed that the parameter B (in Eq. E5) was influenced both by the ratio $\nu = X_M^*/(X_M^* + X_A^*)$ and by X_G^*.

The parameter B can be given by

$$B = B_0 + B_1X_G^* + B_2(X_G^*)^2 + B_3(X_G^*)^3 \qquad \text{(E6)}$$

where B_1, B_2 and B_3 can be obtained from

$$B_i = a_i + b_i\nu + c_i\nu^2 \qquad \text{(E7)}$$

The values of coefficients a_i, b_i and c_i are given in Table E4. The global B-value for a slag containing all three modifiers, CaO, MgO and MnO, can be calculated from separate B-values of individual modifiers. The expression for B_{global} is given by

$$B_{global} = \frac{X_{CaO}B_{CaO} + X_{MgO}B_{MgO} + X_{MnO}B_{MnO}}{X_{CaO} + X_{MgO} + X_{MnO}} \qquad \text{(E8)}$$

The parameter A can be calculated from B_{global} by Eq. (E9) and the viscosity of the slag (in $Nm^{-2}s$) can then be determined by using Eq. (E10)

$$-\ln A_{global} = 0.29B_{global} + 11.57 \qquad \text{(E9)}$$

$$\mu = 0.1[A_{global}T \exp (10^3 B_{global}/T)] \qquad \text{(E10)}$$

For example, for the above BOF slag composition (FeO = 15.0%, CaO = 45.0% SiO_2= 20.0%, MnO = 8.0%, MgO = 4.0%, Al_2O_3 = 3.0%, CaF_2 = 1.4%, P_2O_3 = 3.6%, all are in wt%)

$$A_{global} = 1.1727 \times 10^{-7}$$

$$B_{global} = 15.1335$$

So from Eq. (E10) viscosity of slag is 7.09×10^{-2} kg $m^{-1}s^{-1}$, at 1600°C.

Table E3 Equations for calculating partial molar surface tension for surface-active slag constituents at 1500°C [39]

Slag constituent	$X_i\sigma'_i$ for X < N	N	$X_i\sigma'_i$ for X > N
CaF_2	$-2.0 - 934X + 4769X^2$	0.13	$-92.5 + 382.5X$
Cr_2O_3	$- 1248X + 8735X^2$	0.05	$-84.2 + 884.2X$
Fe_2O_3	$-3.7 - 2972X + 14.312X^2$	0.125	$-216.2 + 516.2X$
P_2O_5	$-5.2 - 3454X + 22178X^2$	0.12	$-142.5 + 167.5X$
S	$-0.8 - 3540X + 55220X^2$	0.04	$-70.8 + 420.8X$

Table E4 Numerical values of coefficient a_i, b_i and c_i for three oxides MgO, CaO and MnO [40]

i	a_i	b_i			c_i		
	All	Mg	Ca	Mn	Mg	Ca	Mn
0	13.2	15.9	41.5	20.0	-18.6	-45.0	-25.6
1	30.5	-54.1	-117.2	26.0	33.0	130.0	-56.0
2	-40.4	138.0	232.1	-110.3	-112.0	-298.6	186.2
3	60.8	-99.8	-156.4	64.3	97.6	213.6	-104.6